Journal of MATERIALS RESEARCH

Invited Review
DOI:10.1557/s43578-025-01549-z

FOUNDATIONS OF MODERN METALLURGY

FOCUS ISSUE

Paradoxes of heterostructured materials

Liliana Romero-Resendiz[1,2,a], Muhammad Naeem[2]

[1] Department of Design and Engineering, Faculty of Science and Technology, Bournemouth University, Poole, Dorset BH12 5BB, UK
[2] School of Metallurgy and Materials, University of Birmingham, Birmingham B15 2TT, UK
[a] Address all correspondence to this author. e-mail: lromeroresendiz@bournemouth.ac.uk

Received: 5 November 2024; accepted: 19 February 2025

Heterostructured materials (HSMs) represent a groundbreaking advancement in materials science, achieving unprecedented combinations of strength and ductility that challenge traditional paradigms. This review explores the state of the art, focusing on foundational concepts such as the Hall–Petch relationship and dislocation dynamics, and correlates these principles with the unique properties of HSMs. The mechanisms behind hetero-deformation-induced strengthening and work hardening are examined in depth, highlighting various types of HSMs and their superior performance. This review critically discusses paradoxes in the field, including the strength–ductility trade-off, the bulk improvement of properties through heterogeneity, challenges in scalability, enhanced performance at cryogenic temperatures, and a high cost-benefit relationship. Future perspectives on HSMs are also outlined, emphasizing emerging trends and potential industrial applications. By integrating foundational concepts with cutting-edge research, this paper provides a comprehensive overview and outlook on the field of HSMs.

Introduction

The Hall–Petch relationship is a cornerstone of materials science, describing how grain size influences the strength of polycrystalline materials as per Eq. (1) [1, 2]

$$\sigma_Y = \sigma_0 + k\frac{1}{\sqrt{d}}, \tag{1}$$

where σ_Y is the yield strength, σ_0 is lattice friction stress (material-dependent constant needed to start the dislocation movement), k is the Hall–Petch slope, and d is the average grain size. According to this principle, reducing grain size increases the material's yield strength by enhancing grain boundary strengthening. Dislocation mechanics, which focuses on the movement and interaction of dislocations in the crystal lattice, further elucidates how materials deform under stress [3, 4]. Dislocation hardening (σ) arises from the mechanism described by Taylor's Eq. (2) [5–7]

$$\sigma_Y = \alpha M G b\sqrt{\rho_S + \rho_G}, \tag{2}$$

where α is a proportionality constant, M is the Taylor factor, which accounts for the crystallographic orientation, G is the shear modulus, b is the Burgers vector, ρ_S is the density of statistically stored dislocations, and ρ_G is the density of geometrically necessary dislocations.

These concepts are crucial for understanding a wide range of polycrystalline materials. However, different microstructural and testing conditions may trigger numerous Hall–Petch variations. Examples of the above are (i) *inverse Hall–Petch relationship* in nanocrystalline (typically below 12–30 nm [8, 9]) and quasicrystalline materials [10], due to the lack of sufficient dislocation activity within such fine grains, as well as dominant grain boundary sliding or grain boundary-mediated plasticity, reducing the efficacy of grain boundaries as barriers to dislocation motion, (ii) high-temperature conditions that induce creep [11], (iii) the effectiveness of grain boundaries in impeding dislocation motion, where high-angle grain boundaries typically provide stronger barriers than low-angle grain boundaries and coherent twin boundaries which leads to *dynamic Hall–Petch relationship* [12], (iv) high strain rate that may cause adiabatic heating and dynamic recrystallization, differing from the quasi-static loading conditions used to derive the original Hall–Petch relationship [13, 14], (v) mechanics controlled by triple grain boundary junctions [15, 16], (vi) complex or anisotropic crystal structures, such as hexagonal close-packed (HCP) metals,

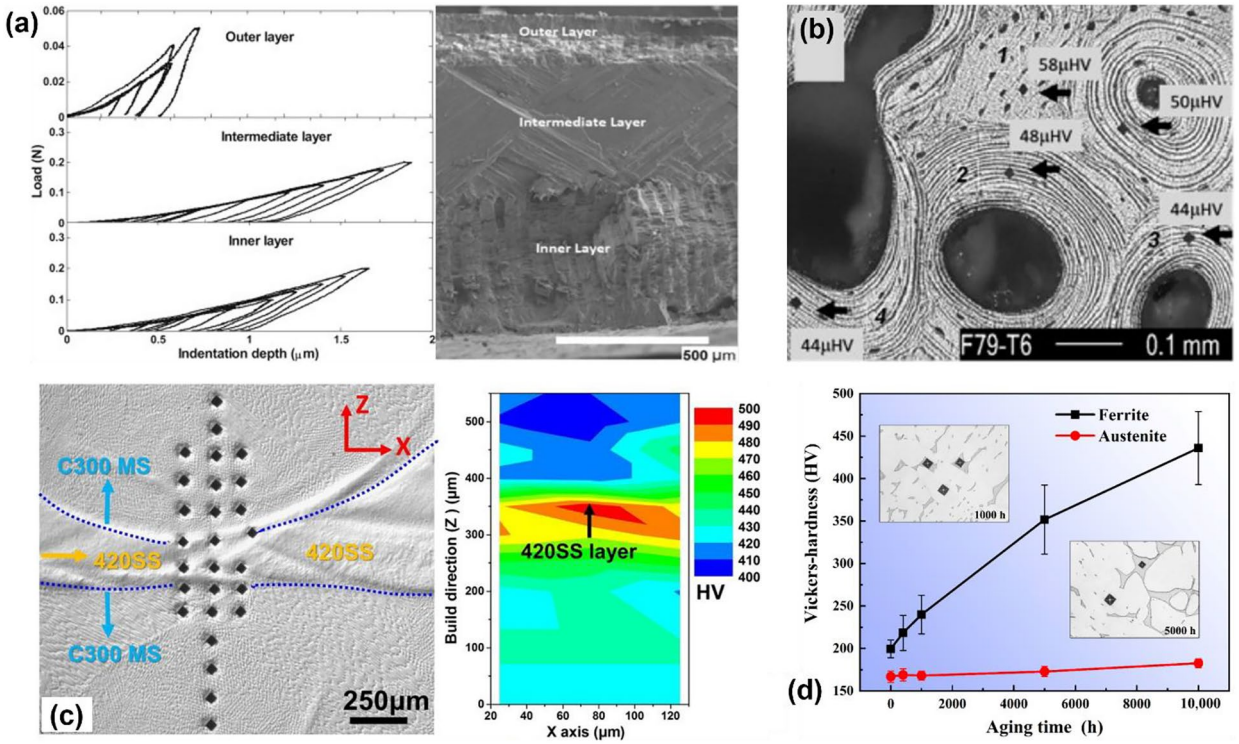

Figure 1: Examples of (a, b) natural and (c, d) man-made materials with high mechanical disparity between coexisting zones. (a) Microhardness depth in different layers of a Charonia lampas lampas shell [20], (b) microhardness at different points of human bone tissue where the lower values correspond to osteons and higher values to interstitial lamellae [21], (c) microhardness mapping across a layered material build by 300 maraging steel and AISI 420 stainless steel [22], and (d) microhardness evolution with aging time in a duplex stainless steels composed of mainly austenite and ferrite phases [23].

certain ceramics, composites and multiphasic materials, where the relationship can be less predictable or the interactions between different phases or defects can dominate mechanical behavior [17], and (vii) dominance of other strengthening mechanisms, such as in heterostructured materials given by grain size heterogeneities [18, 19]. This last situation is the focus of this review, i.e., the mechanical behavior of heterostructured materials, a new class of materials that exhibit superior properties by combining zones with different mechanical characteristics.

Heterostructured materials may also challenge the applicability of Taylor's equation due to microstructural features that are within its limitations. For example, (i) geometrically necessary dislocations, which are abundant in heterostructured materials, contribute differently to strengthening than statistically stored dislocations, (ii) the ignorance of hetero-deformation induced stress, which is significant in heterostructured materials, and (iii) distribution of geometrically necessary dislocation pile-ups concentrated mainly within the softer zones of heterostructured materials, near the interfaces with a high mechanical mismatch.

Despite being a fast-emerging field, heterostructured materials with large mechanical disparities across coexisting zones are commonly found in nature [Fig. 1(a, b)] and engineered materials [Fig. 1(c, d)]. The microhardness profile across different layers of a Charonia lampas lampas shell highlights three distinct regions: the outer, intermediate, and inner layers, each with varying hardness values [Fig. 1(a)]. The accompanying image shows the microstructural contrast among these layers. Figure 1(b) shows the microhardness distribution in human bone tissue, where osteons (lower hardness) and interstitial lamellae (higher hardness) form a composite structure with mechanical inhomogeneity. Figure 1(c) displays a layered material fabricated using 300 maraging steel and AISI 420 stainless steel, with a microhardness mapping clearly demonstrating the sharp transition in hardness across the interface. Lastly, Fig. 1(d) depicts the microhardness evolution over time in duplex stainless steel subjected to aging. The data reveal distinct hardness trends in ferrite and austenite phases, emphasizing their mechanical disparity. These examples illustrate how both nature and engineering exploit mechanical disparities to achieve overall superior properties, making them prime candidates for studying heterostructured materials.

The origin of mechanical disparities in heterostructured materials can be from heterogeneous grain size, crystallographic texture, defects density, or chemical composition [19]. In addition to mechanical mismatch, heterostructured materials must

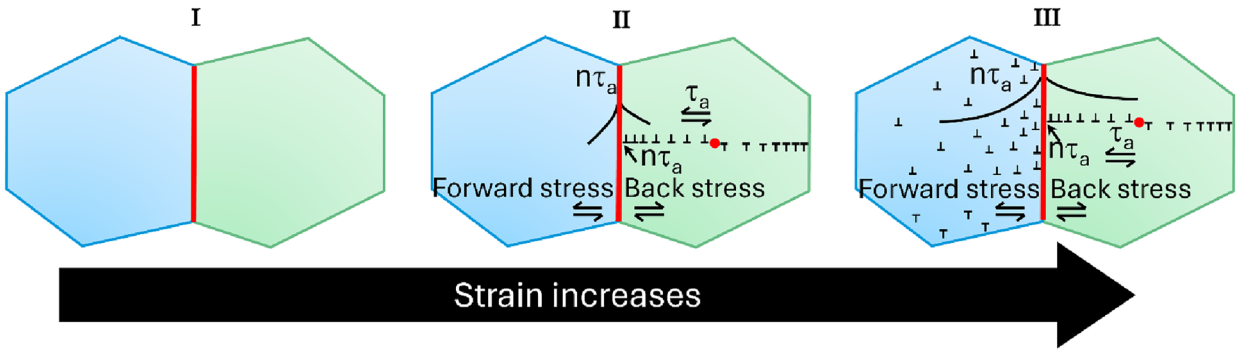

Figure 2: Representation of the three deformation stages (I, II, and III) of heterostructured materials together with the dislocation behavior and stress distribution (black line) from the zone boundary (red line). τ_a is the applied shear stress and n is the number of geometrically necessary dislocations in the pile-up. Red dots represent the dislocation sources.

satisfy specific conditions to enhance the strength–ductility trade-off that limits conventional materials. The fundamentals of heterostructured materials will be briefly covered in "Fundamentals of heterostructured materials" section of this review considering that they have already been deeply described in the literature [18, 19, 24–26]. The central focus of this review is on the paradoxes, i.e., qualities that seem contradictory to the classical knowledge, which have been challenged by the development of heterostructured materials. Four of those paradoxical phenomena, which are based on recent research findings, are described here: (i) Rethinking how we can leverage the very material heterogeneities we usually strive to eliminate, (ii) improvement of the classically accepted strength–ductility trade-off, (iii) taking advantage of smart-selected heterogeneities to develop advanced bulk performance, and (iv) improving toughness under low atomic mobility conditions, such as cryogenic temperatures. Therefore, this paper intends to provide a deep understanding of the physical fundamentals of heterostructured materials and their differences from conventional materials, which can be exploited in vast applications such as biomedical, aircraft, building, optoelectronics, clean energy, and nuclear. Lastly, this review critically discusses the perspectives of this promising field.

Fundamentals of heterostructured materials

Heterostructured materials (HSMs) exhibit remarkable mechanical properties arising from the interaction between their soft and hard zones (Fig. 2). These zones differ significantly in flow stress, leading to a heterogeneous response to applied strain [19]. Soft zones (indicated in green color in Fig. 2), typically coarse-grained (micrometric sized), undergo larger deformations, while hard zones (indicated in blue color in Fig. 2), often nano- or ultrafine-grained, act as barriers to dislocation movement, enhancing material strength [26]. Interfaces between these zones, also known as zone boundaries, are crucial to accommodate strain mismatches by generating geometrically necessary dislocations (GNDs) [27].

The GNDs pile up and create long-range back stress in soft zones and forward stress in hard zones, providing simultaneous extra strengthening and strain hardening, respectively [24]. Together, back and forward stresses generate hetero-deformation-induced (HDI) stress [28]. Therefore, GND pile-ups are a key factor for generating HDI stress and they can be encouraged by activating planar slip and avoiding cross slip. Planar slip can be promoted by low stacking fault energy (SFE), short-range order, high shear modulus, and large atomic size mismatch [26]. Mutual constraining and strain gradient near the zone boundary, i.e., the hard/soft interface, will be accommodated by GND pile-up formation [19, 27]. The strain gradient is triggered by a mechanical property mismatch of at least 100% between soft and hard zones.

The deformation process of HSMs can be divided into three stages, as shown in Fig. 2. Stage I involves the elastic deformation of both soft and hard zones. In Stage II, dislocation slip occurs in the soft zones, while the hard zones remain elastic. This stage is characterized by the accommodation of the strain gradient in the soft regions through GNDs piling up against the zone boundaries, creating back stress. Simultaneously, the hard zones constrain the soft zones, generating forward stress, and leading to strain partitioning. Stage III involves the plastic deformation of both zones, where the interaction between the soft and hard zones continues, enhancing overall strain hardening and strengthening.

HDI stress results in superior strengthening and strain hardening, surpassing that of homogeneous materials [26]. As a result, the yield strength of HSMs often exceeds predictions from the rule of mixtures (ROM). This is due to the significant contributions of HDI strengthening and strain hardening to the material's properties. The interaction between back stress and forward stress does not cancel out overall. Although they neutralize each other at the boundary, they exhibit different profiles

as they move away from it (black line in Fig. 2), which leads to significant HDI strengthening and strain hardening [25].

Although HDI strengthening and strain hardening are major mechanisms in HSMs, their superior properties also result from the cumulative effect of various other strengthening mechanisms [27]. Microstructural defects, such as zone boundaries (interface between soft/hard zones) from multiphase frontiers, multi-order grain sizes, twins, stacking faults, solid solution atoms, and dislocation accumulation, promote diverse strengthening mechanisms. The combined effect of these mechanisms surpasses the expectations from traditional models. Unlike in homogeneous materials, HDI strengthening is crucial for HSMs and must be included in classical models like ROM. The contribution of HDI and synergistic strengthening is nonlinear and necessitates a modification of the ROM to estimate the yield strength as per Eq. (3) [29]

$$\sigma_Y = \Delta\sigma + \sum_{i=1}^{n} f_i \sigma_i, \tag{3}$$

where σ_Y is the yield strength of the entire material, $\Delta\sigma$ represents the synergistic strengthening contribution, and f_i and σ_i are the volume fraction and yield strength of each layer/zone. This can also be expressed as

$$\sigma_Y = \Delta\sigma + \frac{1}{t}\int_0^t \sigma(x)dx, \tag{4}$$

where t is the total thickness/volume of the sample and $\sigma(x)$ is the yield strength of each layer/zone. The origin of $\Delta\sigma$ is also related to the mismatch of Poisson's ratio between coarse and fine regions. Finite element method simulations show a biaxial stress state induced by this mismatch, enhancing dislocation accumulation, activating more slip systems, and resulting in increased strength and ductility [30].

Besides their superior mechanical performance, HSMs hold immense potential across various industrial and technological applications due to their potential combination of mechanical, biological, and chemical properties [19]. These materials can significantly enhance performance in sectors such as aerospace, automotive, biomedical engineering, and nuclear applications. In aerospace, the high strength-to-weight ratio and improved ductility of HSMs can lead to the development of lighter and more durable components [31–33]. The automotive industry can benefit from these properties by producing more efficient and safer vehicles [32, 33]. In the biomedical field, the enhanced biocompatibility and adequate corrosion resistance of heterostructured stainless steels make them ideal for implants and medical instruments [19, 34–37]. The high density of interfaces (subgrains and nano-inclusions) may serve as sinks for He atoms, improving radiation-induced swelling resistance for nuclear applications [38, 39]. Additionally, HSMs may provide superior fatigue, wear resistance, hydrogen embrittlement resistance, and cryogenic mechanical performance, which can extend the lifespan of components in demanding environments, such as in the oil and gas industry, hydrogen economy, or marine applications [40–42]. The versatility and cost-effectiveness of producing HSMs using conventional industrial processes further underscore their potential for widespread adoption in various fields.

Paradoxes of heterostructured materials

Overcoming the strength–ductility trade-off

One of the most striking paradoxes of HSMs is their capacity to achieve both high strength and high ductility [27]. Conventionally, materials that exhibit high strength tend to suffer from reduced ductility, and vice versa. HSMs overcome this trade-off by harnessing HDI strengthening and HDI strain hardening, complementing traditional strengthening mechanisms. Homogeneous alloys also produce HDI stress but its contribution is usually very small due to the lack of high mechanical mismatch interfaces where GND pile-ups accommodate the strain in HSMs. As a result, several HSMs had shown enhanced strength than that predicted by the ROM [43]. Moreover, the combination of multi-order grain sizes results in a deviation from the Hall–Petch relationship [18, 19].

As an example of the above, titanium heterogeneous lamella (HL) structures have shown a remarkable combination of strength and ductility, surpassing their ultrafine-grained (UFG) and coarse-grained (CG) counterparts [44]. The HL structures of Ti were produced by asymmetric rolling and partial recrystallization. They are constituted of soft, micro-grained lamellae embedded within a matrix of hard, UFG lamellae. Extra strengthening in HL structures stems from back stress hardening created at the softer lamellae, which has a mutual constraining with the surrounding hard UFG layers. The high mechanical mismatch between them, together with the mutual geometrical constraints of the crystal lattice, triggers the formation of GNDs to accommodate the strain gradients [45]. If the applied shear stress (τ_a in Fig. 2) exceeds the critical shear stress to activate the Frank-Read dislocation source, then GNDs will be emitted and accumulate at the zone boundary. Considering that the softer zones start deforming before the hard ones, significant GND pile-ups can be expected at the softer lamellae. As these GNDs share the same Burgers vector, they collectively generate a long-range internal stress opposing further dislocation emission from the Frank-Read source [25]. This internal stress counters the applied shear stress, reducing the local stress experienced by the Frank-Read source to below the critical shear stress needed for further dislocation release. Therefore, emitting additional dislocations from the Frank-Read source requires applied stress high enough to overcome both the back stress and the critical shear stress. As a result, long-range back stress acts to resist plastic

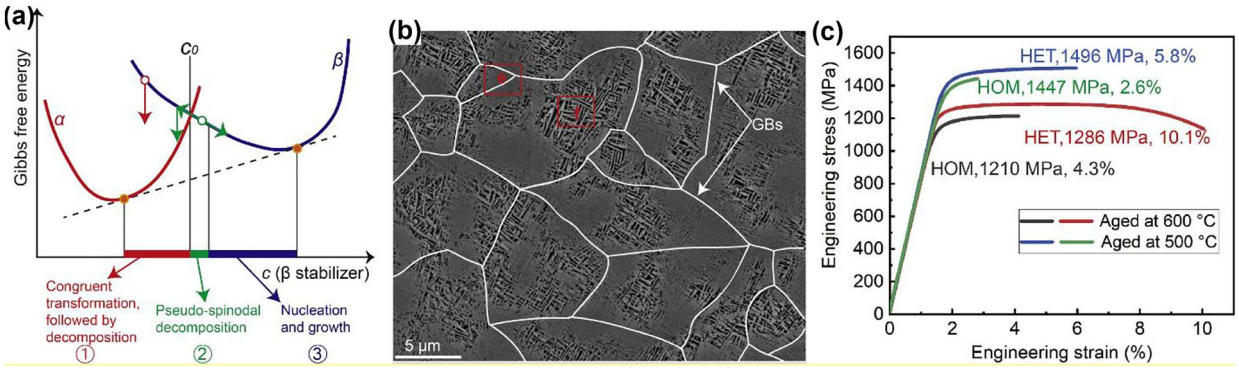

Figure 3: Design, microstructure, and mechanical behavior of the heterostructured Ti-55531 alloy. (a) Schematic diagram of free energy variation in the present phases (α and β) as a function of the β-stabilizer concentration where the red concentration region indicates a congruent β → α phase transformation followed by solute partitioning; the green concentration region indicates pseudo-spinodal decomposition mechanism; and the blue concentration region indicates nucleation-and-growth phase transformation mechanism. As a result, (b) composition modulation led to a heterogeneous distribution of precipitates, with ultrafine α phase predominantly covering the grain boundaries and coarse α phase present within the grains. (c) Improved mechanical properties between heterostructure (HET) and homogeneous (HOM) Ti-55531 alloy [47].

deformation in the soft zone. At the front of the dislocation pile-up, a stress concentration is developed with a magnitude proportional to the number of dislocations in the pile-up ($n\tau_a$ in Fig. 2) [46]. This concentration applies stress on the zone boundary from the soft zone side, which is balanced by forward stress in the hard zone side, effectively aiding the hard zone's deformation. Forward stress functions similarly to the applied stress by driving dislocation slip. At the boundary, the back stress and forward stress are equal in magnitude but opposite in direction. The combined effects of HDI strengthening and HDI hardening result from the interaction between back stress and forward stress providing the HL Ti with a better combination of strength and ductility. The total ductility in the HL structures of Ti was explained in terms of HDI hardening acting synergistically with dislocation hardening [44]. It should be noted that this report from 2015 described only the effect of back stress. However, the same authors redefined in 2019 the additional strengthening and strain hardening observed in HSMs as HDI stress due to the collective action of back and forward stress [28].

Another example is the heterostructured Ti–5Al–5Mo–5 V–3Cr–1Zr (Ti-55531) alloy created by microscale concentration modulations in the β-phase matrix [47]. The HS Ti-55531 alloy was designed to show multiple and simultaneous precipitation mechanisms, i.e., congruent structural transformation, decomposition, and nucleation-and-growth [Fig. 3(a)], that led to coexisting ultrafine and coarse α precipitates as shown in Fig. 3b. As a result, the heterostructured Ti-55531 alloy demonstrated 130% and 6% increments of ductility and ultimate tensile strength compared to its homogeneous counterpart [Fig. 3(c)] [47]. The mechanical properties were improved by reducing strain localization while encouraging dislocation accumulation, twinning, and HDI stress. The significant HDI stress was triggered by the HS Ti-55531 alloy's ability to partition strain between coarse and ultrafine precipitate regions ensuring that the material maintains strength while delaying failure through higher strain hardening.

The HDI stress can be estimated through its close relation to the Bauschinger effect, as both phenomena originate from GND pile-up [48]. The Bauschinger effect, which is the disparity between applied and reversed flow stress, results in a lower compressive yield strength compared to the tensile yield strength, and vice versa [49]. This effect arises because the directional long-range back stress impedes dislocation slip in the tensile direction while facilitating it in the reverse direction [50]. Back stress can account for up to 88% of the flow stress difference attributed to the Bauschinger effect [51]. Consequently, higher HDI stress correlates with a more pronounced Bauschinger effect.

In HSMs, the strain hardening has a major contribution from HDI, unlike homogeneous materials where it is controlled by forest dislocation hardening—mutual trapping and accumulation of statistically stored dislocations (SSDs). Thus, HDI's contribution to overall hardening in HSMs can surpass that of traditional dislocation hardening mechanisms [52]. This has been demonstrated by the higher HDI stress observed due to GND pile-up in heterostructured copper [50] compared to pure copper [53], where the Bauschinger effect is minimal.

An experimental method to estimate HDI stress[1] (σ_{HDI}) during unloading–reloading loops in tensile tests has been proposed as shown in Eq. (5) [54]:

$$\sigma_{HDI} = \frac{\sigma_r + \sigma_u}{2}, \tag{5}$$

[1] HDI stress, i.e., back and forward stress combined, is a term adopted in 2019 [28]. Previous publications including the one reporting Eq. (5) described it as back stress.

where σ_u and σ_r represent the unloading and reloading yield stress, respectively. By this method, one can foresee that the reloading stress will always surpass the unloading stress due to the effect of HDI stress. Equation (5) assumes reversibility of the GND pile-up during the unloading–reloading process, maintaining approximately constant HDI stress. However, this assumption might not hold for materials with high HDI stress, where σ_r could be lower than σ_u. To address this issue, it is recommended to not unload completely to zero stress and rather commence reloading above a specific stress level that aligns with the assumptions of Eq. (5) [27].

As an example of the above, homogeneous oxygen-free copper [Fig. 4(a)] was subjected to surface mechanical attrition treatment to produce a gradient structure [GS, Fig. 4(b)] heterostructured material [50]. The monotonous tensile loading is shown by the black curve in Fig. 4(c) and (d), while the tensile-compressive tests (with different loading pre-strains) are shown by long-dashed lines in Fig. 4(c) and (d). The flow stress is indicated by circles and the reverse yield strength by squares in the tensile-compressive curves of Fig. 4(c) and (d). In the CG copper, both the forward and reverse yield stresses increased with applied strain, indicating typical forest dislocation hardening due to an increase in dislocation density with plastic strain. This non-directional hardening influences both forward and reverse yield stresses, resulting in minimal Bauschinger effect. In contrast, the GS copper showed an unusual increment of forward flow yield strength, while reverse yield strength decreased due to its pronounced directional back stress that induced a significant Bauschinger effect. The heterogeneous interfaces—given by different grain size orders—generate high strain gradients to be accommodated by GNDs, which produce directional HDI stress. The HDI stress in GS Cu restricts dislocation motion in tension while facilitating it in compression.

Bulk properties through heterogeneity

Another paradox lies in achieving bulk mechanical properties through heterogeneous microstructures. Controlled heterogeneity in HSMs leads to superior performance because the different zones work synergistically to enhance overall properties. For

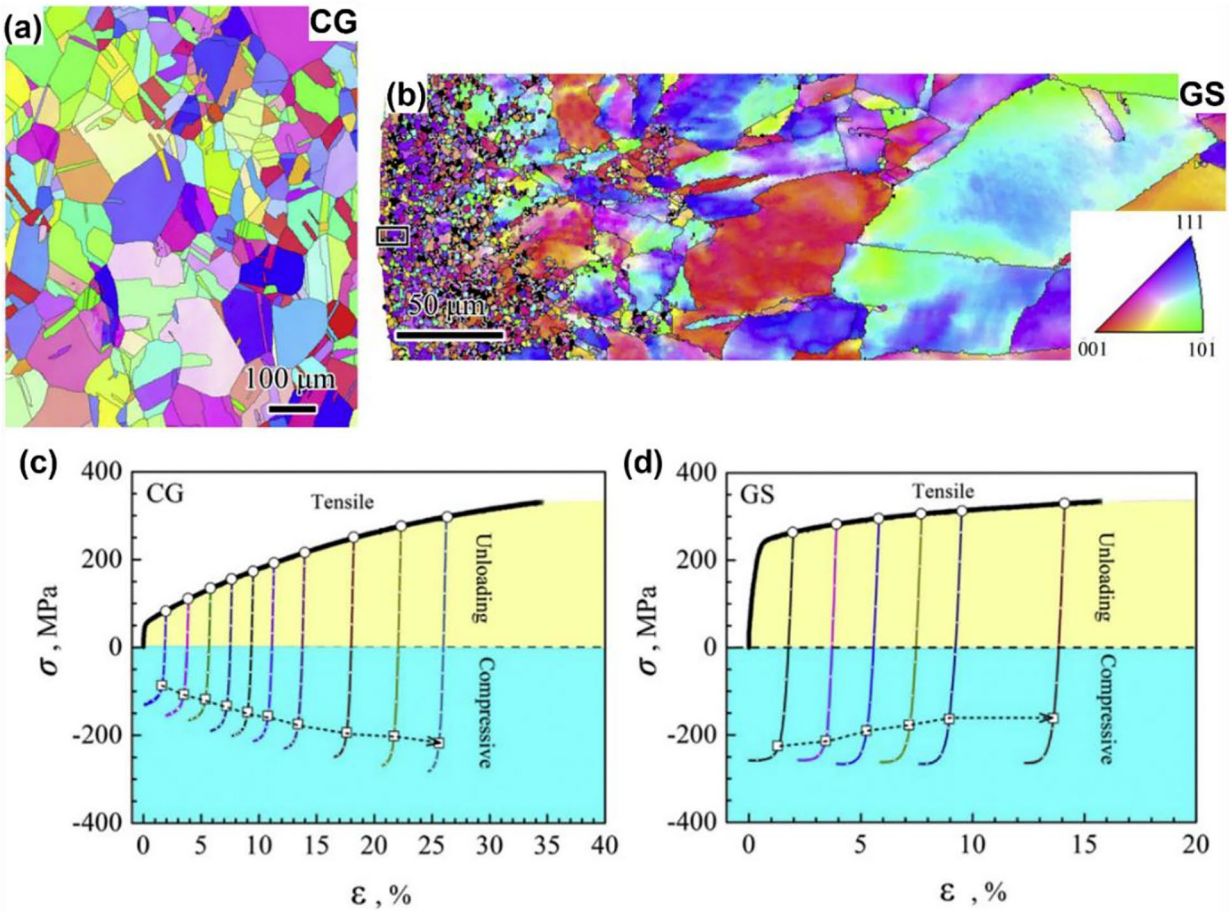

Figure 4: EBSD maps of (a) coarse-grained (CG) Cu and (b) gradient structure (GS) Cu, as well as tensile-compressive stress–strain curves for (c) CG Cu and (d) GS Cu [50].

instance, the presence of soft and hard zones within a material can help to balance strength and ductility.

The nonlinear contribution of $\Delta\sigma$ indicates an optimal volume fraction or thickness of fine zones that maximizes mechanical properties [30]. Therefore, an optimal fraction of soft and hard zones may maximize the synergy between GND pile-up and dislocation accumulation. Experimental approaches have optimized the volume fraction of fine zones in harmonic structured 304L stainless steel and copper to around 40% [55, 56]. Dual-phase stainless steel and manganese steel, examples of multiphase materials, achieved superior properties at ~ 30 vol.% of martensite (α') [57, 58]. For 316L stainless steel, a combination of 30 vol.% nano-grained and 10 vol.% nano-twinned zones achieved the best optimized strength–ductility combination [43]. Similarly, prolonged transformation-induced plasticity (TRIP), HDI strengthening, and HDI strain hardening were optimized in a gradient 304 stainless steel with ~ 30 vol.% α' [59]. In gradient interstitial-free steel, HDI strengthening was optimized at a fine zone volume fraction of ~ 50% [30]. For a shell fraction of 41% in harmonic structured 304L, the ultimate tensile strength peaks at 744 MPa, with a slight decrease observed at higher shell fractions [55].

Besides the volume fraction of soft zones, their distribution is also important for designing HSMs. The separation between zone boundaries, i.e., hetero-interface spacing, is one of the key parameters to be controlled. Layered structure Cu-bronze materials were designed to evaluate the effect of hetero-interface spacing on its mechanical behavior [Fig. 5(a)] [60]. Comparable chemical, hardness, grain size, and crystallographic heterogeneities across the interfaces of the different samples allowed separating the contribution from variable hetero-interface spacing. The existence of a GND density gradient varying with the distance from the hetero-interface was shown. As shown in Fig. 5(a), the interface-affected zone, given by the highest GND density, extends a few micrometers. The extension of the interface-affected zone was similar within different samples regardless of the differences in interface spacing (given by the layer thickness). Thus, there is a distance-dependent strain gradient. Conversely, the hardening capacity within the interior of the layers remained consistent across the samples. Therefore, the density of hetero-interfaces is a key factor in increasing the GND pile-up density and, consequently, HDI strengthening and HDI strain hardening. It is hypothesized that interface spacing should be of at least the interface-affected extension to provide sufficient space for GND accumulation. This hypothesis was validated by a layered Cu-bronze structure, comparing interface spacings from 3.7 to 125 μm as shown in Fig. 5(b) [61]. The optimal balance of yield strength and ductility was achieved at a spacing of about twice the interface-affected zone (~ 15 μm), preventing overlap between the extension from each

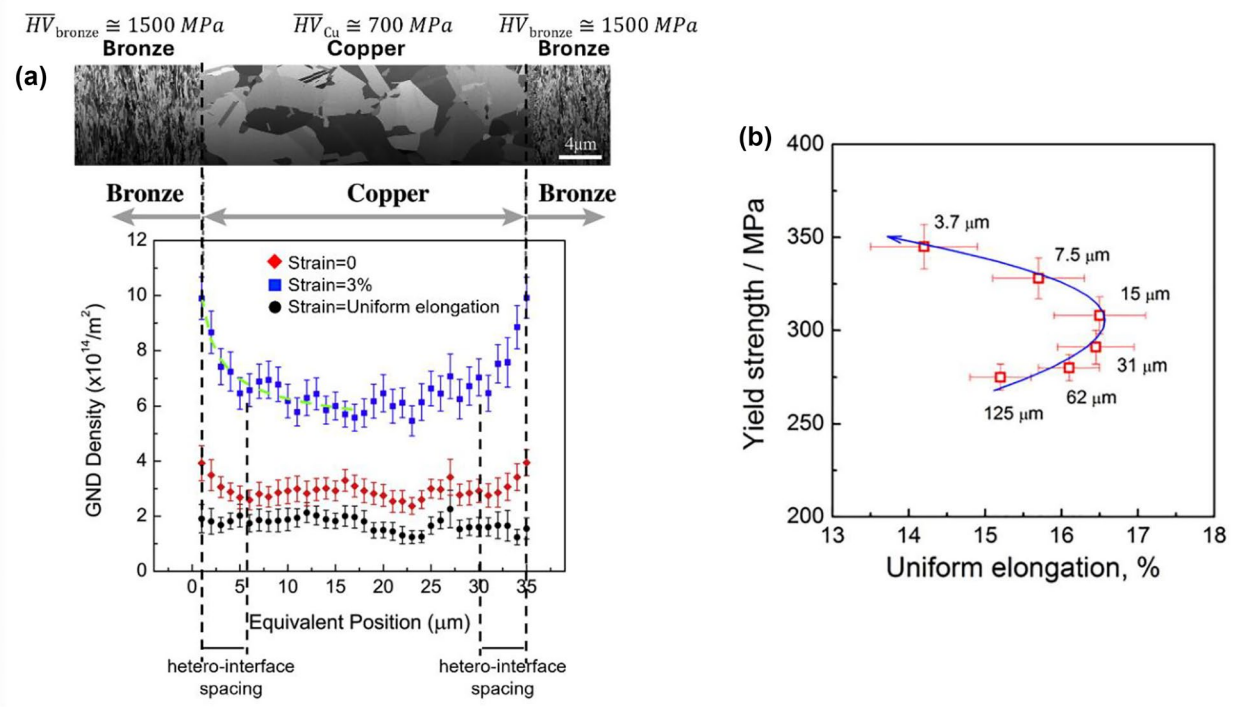

Figure 5: Extension of the interface-affected zone given by the higher GND density and its effect on the strength–ductility trade-off of a layer-structured Cu-bronze heterostructured material. (a) Averaged GND density in the Cu layer as a function of the distance from the interfaces at different strain levels, which indicates the extension of the interface-affected zone by a few micrometers [60]. (b) Strength–ductility relationship as a function of the interface spacing, where an interface spacing of about 15 μm seems to provide the best combination of mechanical properties [61].

hetero-interface edge. When zones overlap, HDI stress generation may be limited; if the spacing is too large, insufficient HDI stress develops to enhance mechanical properties. If the spacing is smaller than twice the interface-affected zone, GND pile-up may be restricted, reducing HDI stress. Therefore, the ideal spacing maximizes HDI strain hardening and strengthening, optimizing mechanical performance. Future studies should model the required fraction and spacing between zones to maximize HDI stress in different HSMs.

Scaling up with enhanced performance

Scaling up the production of HSMs while maintaining their unique properties poses a significant challenge. Taking advantage of conventional low-cost and accessible manufacturing technologies, such as rolling and heat treatments, is a feasible way to produce cost-efficient HSMs [19, 37]. Moreover, advancements in manufacturing technologies, such as additive manufacturing, are paving the way for large-scale production of interdisciplinary HSMs [62]. Additive manufacturing allows for precise control over microstructural features, ensuring that the exceptional properties of HSMs are retained even at larger scales.

Selecting low-cost and scalable thermo-mechanical processes to produce HSMs is recommended to exploit current infrastructure, boosting a smooth transition for their industrial applications. This feasibility arises from the ability to design new combinations of HSM using conventional thermo-mechanical bulk or surface processing methods as indicated in Fig. 6. Examples include surface nanostructuring [63–66], heat treatments [67], severe cold rolling and heat treatments [37, 43, 44, 68–71], severe plastic deformation (SPD) [72–74] or SPD combined with heat treatments [26, 75–77], additive manufacturing [78, 79], powder metallurgy [33], or hybrid techniques [80]. Comparative details on the microstructure and properties of HSMs obtained by different fabrication routes can be found in the literature [19, 27].

Enhanced performance at cryogenic temperatures

Recent studies have demonstrated that HSMs exhibit both increased strength and ductility at cryogenic temperatures, outperforming their properties at room temperature. The key mechanisms driving this improvement include HDI strengthening and twinning, both of which are particularly effective at low temperatures [81–87]. The strain mismatch generated at soft/

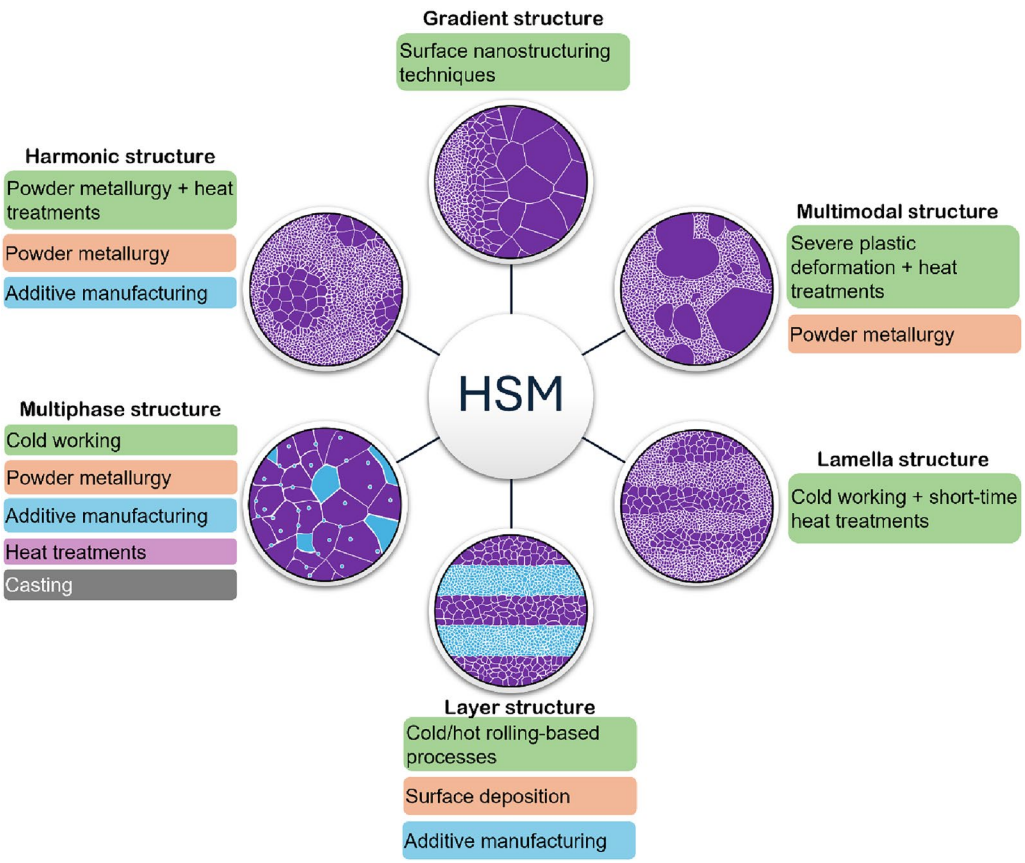

Figure 6: Classification of heterostructured materials (HSMs) and main fabrication methods.

hard interfaces promotes HDI stress, which further promotes the formation of GNDs and twins [83, 85]. HDI stress is amplified at cryogenic temperatures, enhancing the HDI effect and leading to superior mechanical properties [84, 85].

Cryogenic temperatures favor the accumulation of GNDs at the zone boundaries between soft and hard zones [84, 85]. These dislocations generate long-range back stress in the soft zones and forward stress in the hard zones, i.e., HDI stress. HDI enhances the overall yield strength and strain hardening of the material. Moreover, at cryogenic temperature, the activation energy for twinning decreases, making it a major deformation mechanism [88]. The high stresses near zone boundaries promote the formation of twins [83]. These twins act as barriers to dislocation motion, enhancing strain hardening and delaying necking, thereby improving ductility. Furthermore, the difference in Poisson's ratio between the coarse and fine zones induces a biaxial stress state during deformation [83]. This biaxial stress enhances dislocation interaction and accumulation, activating more slip systems and increasing the strength of the plastically deformed layers.

As an example, a heterostructured CrCoNi medium entropy alloy comprising deformed substructures (hard zones) and recrystallized grains (soft zones) significantly improved at cryogenic temperatures [83]. At 77 K, the alloy exhibited a yield strength of 1480 MPa and a uniform elongation of 28%. In comparison, the heterostructured CrCoNi at room temperature resulted in a yield strength of 1080 MPa and 17% uniform elongation. Heterostructured CrCoNi showed a remarkable improvement of mechanical properties from room to cryogenic temperatures compared to the ultrafine homogeneous CrCoNi with only 2% of uniform elongation and yield strength of about 1000 MPa [83, 89].

The temperature effects the SFE tremendously, i.e., lowering of temperature reduces the SFE, thus activating additional deformation mechanisms, e.g., formation of stacking faults and deformation twinning in the above CrCoNi case. It can also trigger martensitic phase transformation due to the more efficient formation of nucleation sites like twins, stacking faults, and metastable intermediate phases [90]. As shown in Fig. 7(a), massive strain-induced $\gamma \rightarrow \varepsilon \rightarrow \alpha'$ phase transformation has been demonstrated in heterostructured stainless steel under cryogenic conditions while being absent at room temperature [Fig. 7(b)] [89]. Phase transformation, together with strain partitioning, was responsible for the 35% higher yield strength and fourfold higher ductility at 77 K compared to 293 K [89]. Figures 7(c) and (d) evidence the superior strength–ductility trade-off achieved by the heterostructured stainless steel under deformation at 77 K compared to 293 K and homogeneous stainless steels over a broader temperature range.

A recent in situ study with neutron diffraction on the heterostructured CrCoNi at 77 K has shown evidence of martensitic phase transformation from FCC to HCP phase during deformation (Fig. 8) [42]. Although the HCP phase is present in a small amount, the in-situ neutron diffraction was able to capture it which was not observed in the post-mortem study [83]. The alloy showed a uniform elongation of ~ 34% along with a yield strength of ~ 1250 MPa [Fig. 8(a)] [42]. The improved mechanical behavior under cryogenic conditions was a result of synergistic strengthening and strain hardening mechanisms, including martensitic phase transformation promoting significant TRIP, increased stacking fault probability indicating the formation of high density of planar faults, HDI stress triggered by the high density of GND pile-ups, and traditional accumulation of SSDs. As a result, the heterostructured CrCoNi alloy demonstrated an improved strength–ductility trade-off compared to homogeneous CrCoNi alloys at room or cryogenic temperatures from the literature [Fig. 8(b)].

The sequential activation of the abovementioned strengthening and strain hardening mechanisms in the heterostructured CrCoNi alloy at 77 K is shown in Fig. 8(c) [42]. During stage I, the deformation initiated in the softer regions ahead of the harder ones, causing GND accumulation in the softer micrometric (recrystallized and ultrafine-grained) areas. Meanwhile, planar faults (PF) and total dislocation density (ρ) increased, with the latter attributed to the concurrent rise in GNDs and SSDs. During stage II, the density of these defects continued to increase, resulting in the first stable region of the strain hardening rate (SHR). Stage III is marked by a reduction in the planar fault formation, as evidenced by a decrease in the stacking fault probability (SFP) slope from 17 to 15%. During stage IV, a significant density of planar faults has accumulated and overlapped, providing nucleation sites for the FCC → HCP phase transformation. The combined effect of TRIP and a more rapid increase in dislocation density, reflected by an increase in slope from approximately 28 to 48×10^{15} m^{-2}, led to the second stable region of the strain hardening rate. Finally, defect saturation occurred in stage V, culminating in the onset of necking. These recent examples of CrCoNi and stainless steel demonstrate that HSMs overcome the strength–ductility trade-off not only at room temperature but also under cryogenic conditions [42, 83, 89].

The improvement of both strength and ductility at cryogenic temperature is not limited to just FCC structured materials. Recently, a similar behavior has been reported for the commercially pure heterostructured Ti at 77 K which has an HCP structure [84]. The heterostructured Ti showed the higher yield strength (~ 1200 MPa) and the uniform elongation (~ 20%) at 77 K, surpassing both traits than the homogeneous fine-grained and the ultrafine-grained Ti at 77 K [84].

Despite the above impressive behaviors, most of the mechanical performance studies of HSMs at cryogenic temperatures have been carried out in FCC matrix materials, making it unclear if the better mechanical performance is

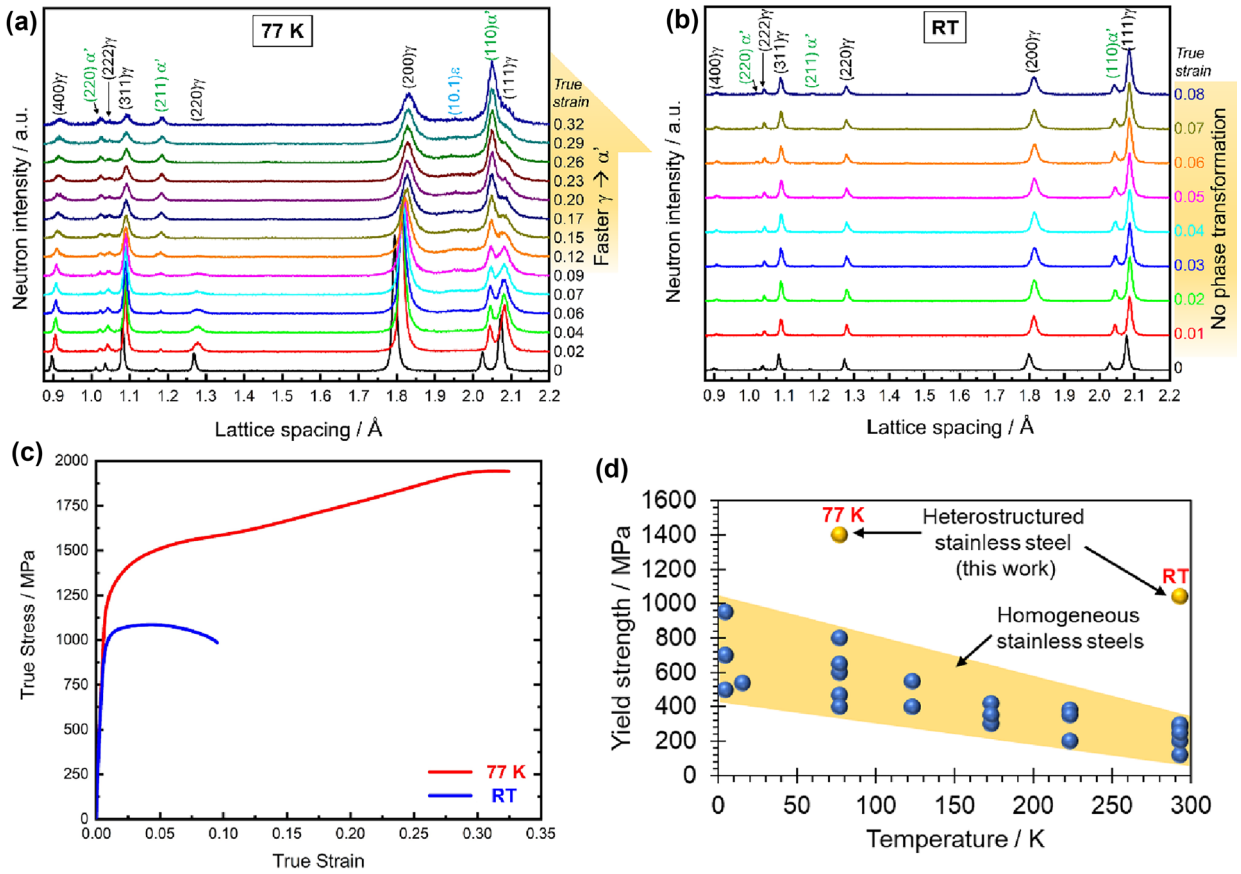

Figure 7: Phase evolution and mechanical behavior of heterostructured stainless steel during in situ neutron diffraction tensile testing at 77 K and room temperature (RT, 293 K). Diffraction patterns along the loading direction highlighting the $\gamma \rightarrow \varepsilon \rightarrow \alpha'$ phase transformation during deformation at (a) 77 K and (b) the absence of phase transformation during deformation at RT. The superior mechanical behavior of the heterostructured stainless steel at cryogenic temperature is highlighted by (c) tensile stress–strain curves and (d) comparison with conventional (homogeneous) stainless steels with deformation temperature [89].

due to the nature of the FCC structure, the heterostructures or the synergy of both features. Homogeneous FCC materials, such as Al alloys, stainless steels, and high-entropy alloys, have shown improved strength–ductility trade-off due to the activation of multiple deformation mechanisms and decrease of SFE at low temperatures [91–96].

The improved mechanical properties under cryogenic conditions make HSMs attractive for applications in extreme environments, such as aerospace, hydrogen economy, cryogenic storage, and natural resources extraction. The further mechanical improvement of HSMs at cryogenic temperatures has been demonstrated in materials as accessible and widely applied such as stainless steel [89] to emerging materials like multi-principal element alloys [42]. Hence, this field has the potential to be explored for materials with a variety of crystal structures, as well as for atomistically understanding the effect of cryogenic deformation on the heterostructure configuration.

Balancing low cost and high efficiency

The typically accepted assumption is that the cost is a credible suggestion for efficiency [97]. However, HSMs can be produced at a low cost and provide a broad platform of benefits beyond mechanical resistance. Their low fabrication cost is based on exploiting conventional thermo-mechanical technologies (Fig. 6) that avoid extra costs for purchasing and installing new fabrication infrastructure [25]. Moreover, utilizing the current infrastructure also encourages a smooth and faster transition of HSMs from laboratory to large-scale industrial production. For example, several heterogeneous lamella structures have been produced by conventional cold rolling and short-time heat treatments. This strategy has improved up to 4 times the yield strength (140 up to 580 MPa) while keeping 7–13% uniform elongation for conventional Cu-30Zn brass through accessible rolling and 10–30 min annealing [98]. Low-cost production together with high mechanical efficiency provides an alternative to decrease the current environmental impact of different metals and alloys. This also highlights that the HSM strategy

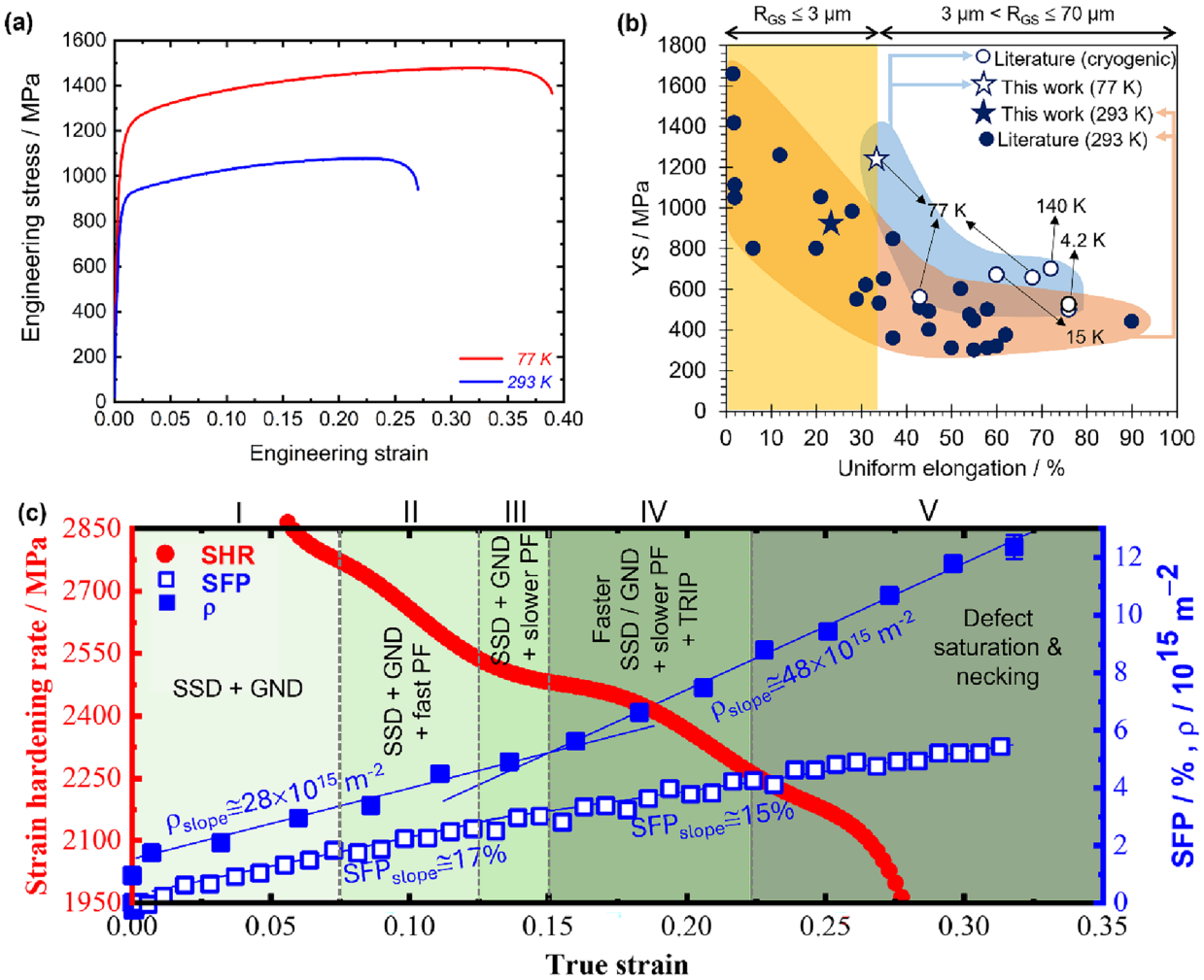

Figure 8: Improved mechanical behavior of the heterostructured CrCoNi at cryogenic temperature (77 K) compared to room temperature (293 K) demonstrated by (a) higher strength and ductility, (b) improved strength–ductility trade-off compared to other CrCoNi alloys from the literature with different ranges of grain size (R_{GS}), where cryogenic and room-temperature data points are indicated in white and blue filled symbols, respectively. (c) Sequential activation of deformation mechanisms at 77 K, including the trends for strain hardening rate (SHR), stacking fault probability (SFP), and total dislocation density (ρ) as a function of true strain [42].

exploits microstructural control to produce stronger and durable materials without the need of substituting accessible elements with more expensive, conflict-sourced, or heavier elements.

The superior strength of HSMs is expected to increase the lifespan of current industrial components made of homogeneous materials. Extending the lifetime, i.e., the average duration of their use, prolongs the conservation of metals and alloys in the economy, increases the generated value to users, and reduces their potential environmental impact [99]. This approach could also contribute to lowering greenhouse gas emissions from the metal production industry, which accounts for ~ 10% of global emissions [100]. The exploitation of current technologies for HSMs production represents an advantage for faster positive environmental effects compared to new technologies that must undergo development and commercialization [100].

Regarding efficiency, HSMs can be combined with interdisciplinary properties for wide applications, including biomedical [78, 101], structural [102], green-energy [103, 104], automobile [105–107], cryogenic [84, 108], and optoelectronic materials [109, 110]. This facilitates a broad impact and acceptance in the global market. For example, stainless steel biomedical components, such as molar bands in orthodontic treatments and hypodermic needles, report potential health risks that can be addressed by the HSMs approach. It has been reported that orthodontic molar bands cause temporal or permanent teeth damage [111, 112], which can be addressed by antimicrobial metallic particles-bearing stainless steel. On the other hand, hypodermic needles used for anesthesia, blood administration, transfusions, and vaccinations may break during clinical procedures because of sudden movement of the patients, medical

mistakes, or poor mechanical behavior [113–116]. This risk may be addressed by a heterostructured design that adjusts the soft and hard zone fractions, as well as their mutual constraining, for an optimized contribution from HDI stress and other synergistic strengthening and strain hardening mechanisms. Targeting this societal need, different stainless steels have combined bulk antimicrobial properties with improved mechanical behavior given by heterogeneous microstructures [37, 69, 117, 118].

An example of the above is shown in Fig. 9 where heterostructured and antimicrobial stainless steel was fabricated by four different routes (R1 to R4 in Fig. 9), i.e., combinations of cold rolling and heat treatments [37]. Heterogeneous lamella structures consisting of softer lamellar coarse grains (LGC) surrounded by harder UFG zones were obtained as depicted by the representative Fig. 9a. Adding 3 wt.% of copper provided conventional 316L stainless steel [316L in Fig. 9(b)] with antimicrobial properties that kill from 55 to 72% of Escherichia coli bacteria in 6 h either in the heterostructured (R1 to R4 in Fig. 9) or homogeneous [IC in Fig. 9(b)] conditions. However, heterostructured 316L + 3Cu showed better combinations of strength and ductility than the homogeneous 316L + 3Cu with coarse or fine grain sizes [Fig. 9(c) and (d)]. As shown by representative stress–strain curves in Fig. 9(c), the heterostructured 316L + 3Cu has similar values of yield strength compared to the 80% cold rolled 316L + 3Cu (80CR, homogeneous fine-grained condition) but up to 90% higher uniform elongation. Figure 9(d) displays a comparison of several heterostructured and homogeneous 316L + 3Cu conditions highlighting the improved mechanical behavior of heterostructured materials compared to the typical banana curve followed by homogeneous materials. Future work should focus on HSMs life cycle assessments, as well as material flow, circular economy, and input–output analyses. The previous analyses include the identification and reduction of metal losses along supply chains, environmental impact, potential recycling pathways, etc.

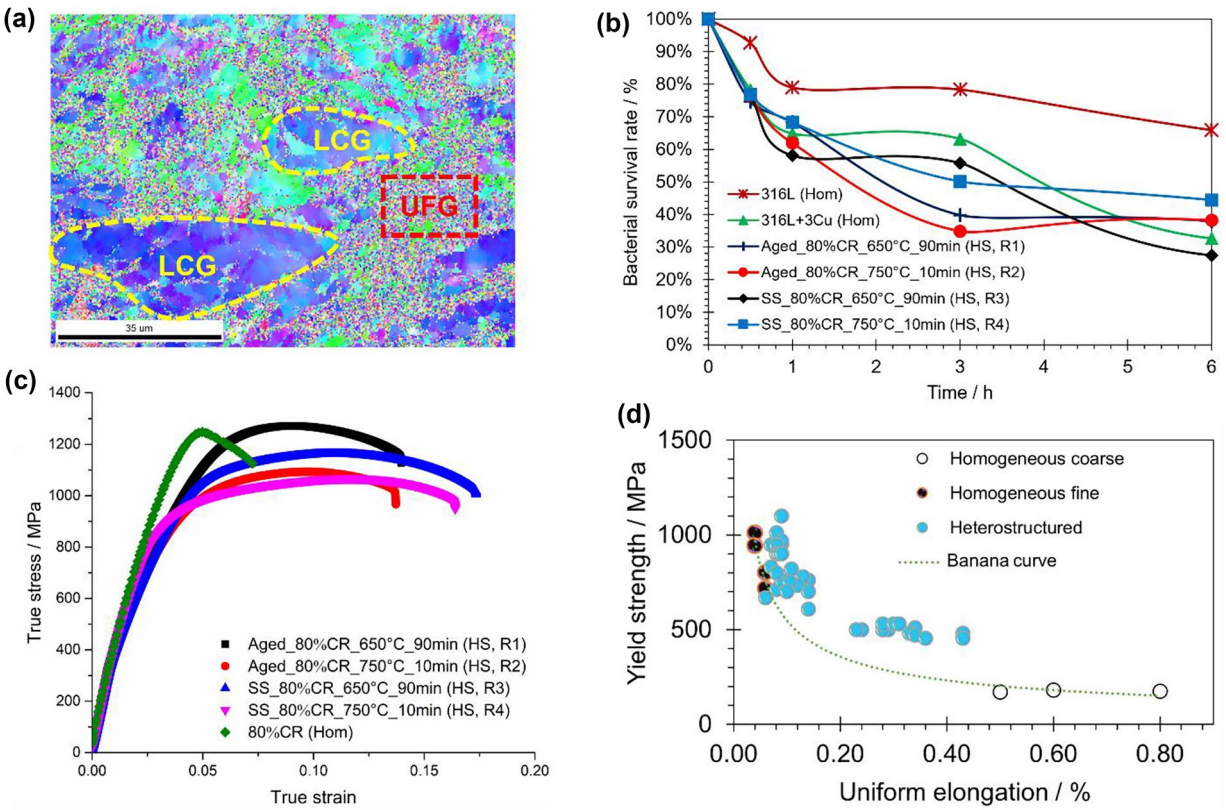

Figure 9: Comparison of antimicrobial and mechanical properties between heterostructured and homogeneous 316L stainless steel with addition of 3 wt.% Cu. (a) Representative microstructure of the heterostructured and antimicrobial stainless steel given by soft lamellar coarse-grained (LCG) regions surrounded by harder ultrafine-grained (UFG) regions [37], (b) Comparison of antimicrobial capacity given by the bacterial survival rate of the control 316L without copper, and homogeneous (Hom) and heterostructured (HS) 316L + 3Cu produced by different thermo-mechanical routes R1-R4 (adapted from [37]), (c) Representative tensile stress–strain curves of the antimicrobial homogeneous (produced by 80% cold rolling) compared to the heterostructured and antimicrobial stainless steels (adapted from [37]), and (d) overview of the improved strength–ductility trade-off of heterostructured 316L + 3Cu compared to the homogeneous 316L + 3Cu, which are subjected to the typical banana curve.

Perspectives on heterostructured materials

The Hall–Petch relationship, the Bauschinger effect, and dislocation mechanics provide a foundational understanding of how HSMs achieve superior mechanical properties. HSMs challenge traditional paradigms by simultaneously enhancing strength and ductility, achieving bulk and large-scalable properties through heterogeneous structures, and demonstrating exceptional performance at cryogenic temperatures.

Future research in the fast-emerging field of HSMs, summarized in Fig. 10, is likely to focus on a deeper understanding of the mechanisms of HDI strengthening and HDI strain hardening. Advances in grain boundary engineering, dislocation dynamics, and real-time (in situ) studies will be crucial in fostering the reproducibility and computational modeling as well as predictive machine learning of HSMs. More sophisticated multi-scale models are essential to better understand the interplay between GNDs and different interfaces with diverse mechanical mismatches. Developing hybrid methods that integrate finite element modeling, molecular dynamics, and crystal plasticity simulations will enhance the predictive power for HSM behaviors, especially under complex loading conditions and temperature ranges. In particular, modifications to the Taylor hardening equation or Hall–Petch relationship to account for nonlinear strain gradient effects and HDI stress could be beneficial. For example, titanium HL structures—HL60 and HL80—showed high yield strength due to dislocation and HDI strengthening mechanisms, contrary to the decrease predicted by the Hall–Petch (Eq. (1)) and Taylor (Eq. (2)) equations [44]. Recrystallized zones with nearly zero dislocation density coexist with significantly recovered non-recrystallized regions, yet UFG (cold rolled), HL60, and HL80 samples exhibit similar yield strengths.

Traditional constitutive models, which were developed primarily for homogenous materials, require adaptation to accurately represent HSMs. Data-driven techniques, such as machine learning and artificial intelligence, offer the potential for discovering new relationships between microstructural attributes (e.g., grain size and phase distributions, fraction of hard and soft zones, etc.), chemical composition, and mechanical performance. Implementing Bayesian optimization or reinforcement learning within HSM datasets could uncover unexpected synergies between phases and assist in optimizing microstructure for specific applications. An example of the use of this approach is the work by Wahl et al. [119], which advances machine learning–driven design of heterostructures by integrating Bayesian

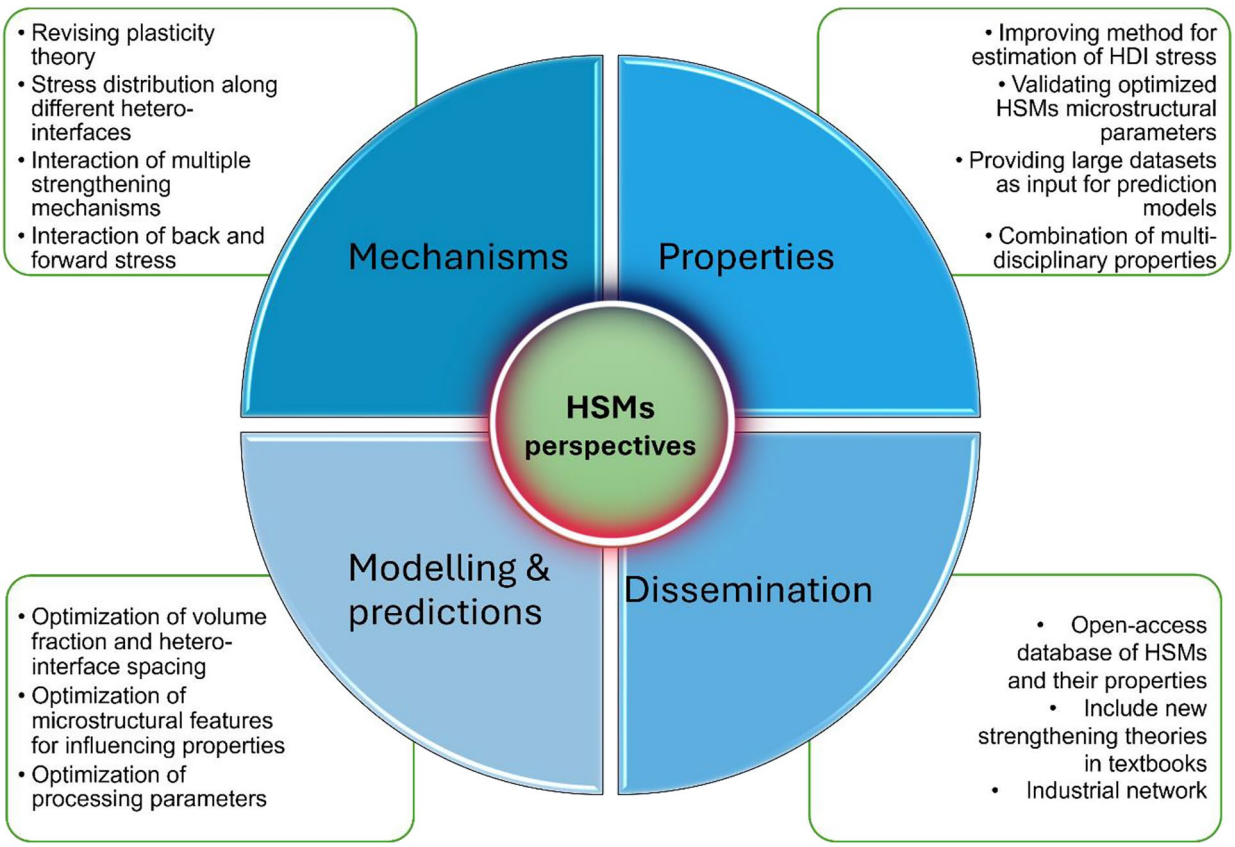

Figure 10: Recommended perspectives for heterostructured materials field.

optimization with a feedback loop that refines experimental design based on synthesis and imaging of nanomaterials. This approach achieves efficient discovery of complex polyelemental nanoparticles that challenge traditional intuition. The Bayesian optimization framework dynamically learns optimal compositions and structural motifs, leading to rapid, targeted synthesis of previously unknown nanostructures. Another example of Bayesian optimization for predicting microstructure-based properties of dual phase steels includes the work of Jung et al. [120]. Similar methodologies may be foundational for materials research, including HSMs, providing scalable, interdisciplinary tools to navigate vast microstructural possibilities and optimize performance across applications [121].

Despite the above, data-driven learning prediction and control may be limited by the trade-off between time, expense, and accuracy, where the cost of large datasets might exceed the value of their provided insights [121]. For example, large data sets may be needed for deep learning techniques such as neural networks to elucidate complex fabrication-structure-property relationships. Therefore, providing open raw datasets and performing high-data volume characterization and experimentation (e.g., synchrotron or neutron scattering techniques) may support accelerated HSMs design and fabrication. In situ bulk characterization techniques can also provide information on the dynamic interactions of defects within heterogeneous zones to be accounted for during modeling and prediction. Producing libraries with large volumes of HSMs data would also foster their prediction.

Regarding the estimation of HDI stress, it assumes reversible GND structures during the unloading–reloading cycle, which might not satisfy materials with high HDI stress. Developing improved methods or systematic corrections for estimating HDI stress remains a promising area for future research, which will also enhance the understanding of the properties of HSMs.

Interface boundaries play a critical role in HSMs by providing pathways for dislocation blocking, transmission or modulation. Investigating how different interface boundary characteristics—such as misorientation angles, coherency, local chemical fluctuations that lead to possible local SFE fluctuations, etc.—contribute to the mutual constraining between soft-hard interfaces and interaction with high density of GNDs pile-ups in HSMs is key. Additionally, expanding research into the impact of nanoscale boundary segregation could be useful in HSMs for applications demanding high thermal stability. Control over interface boundary parameters could be achieved through targeted fabrication methods, heat treatments or deformation techniques, enabling tailored mechanical properties.

Additionally, the development of new or improved fabrication techniques will enable more complex and effective HSMs to meet interdisciplinary needs, e.g., biocompatibility, biosafety, energy-harvesting, self-sustained optoelectronic, and catalytic materials. Innovate fabrication can target a more precise control of microstructural gradients. Techniques like accumulative roll bonding, additive manufacturing, and surface mechanical attrition treatment have demonstrated potential [22, 60, 65], but further refinement is necessary. Specifically, more accurate control of grain size and hard-soft zone spacing can result in optimized properties of HSMs.

Fatigue performance is another relevant topic to comprehend for heterostructured materials. Several studies report that heterostructures improve fatigue life by promoting synergistic interactions between hard and soft regions, which enhances strength and ductility while suppressing crack growth through mechanisms like crack deflection, promoting secondary hardening stages, and higher strain homogeneity [122–124]. For instance, gradient nanostructured 316L stainless steel and graded grain TWIP steel exhibited enhanced fatigue resistance by effectively distributing strain and delaying crack propagation [122, 123]. Conversely, other research shows that heterostructures may reduce fatigue life under specific conditions. Harmonic structured Ti–6Al–4 V, for example, displayed higher crack growth rates and lower fatigue thresholds due to diminished roughness-induced crack closure by the presence of fine-grained regions [125]. Similarly, single-phase heterostructured 316L stainless steel experienced reduced low-cycle fatigue life due to strain partitioning, which concentrated plastic deformation in soft grains, accelerating crack initiation [126]. The controversy arises from the complex interplay between microstructural factors such as grain size, volume fraction, distribution of soft and hard zones, and mechanical incompatibility of the hard and soft phases. While heterostructures generally enhance static properties, fatigue involves cyclic loading where localized strain accumulation can either impede or promote failure, making fatigue behavior highly context-dependent. Thus, the effectiveness of heterostructured materials in fatigue applications depends on balancing these microstructural factors and should be systematically studied for better fatigue life predictions.

The unique properties of HSMs make them ideal for a wide range of industrial applications. In the automotive, structural, and aerospace industries, HSMs can lead to lighter and stronger components, improving fuel efficiency, cost-effectivity, and reducing the quantity of material needed. Besides, increasing the mechanical properties can be translated into longer service life that decreases the metallic waste together with their reduced environmental impact. In the biomedical field, HSMs can be used to create more durable, biosafe, and biocompatible implants. Tailoring compositions and designing heterostructures that incorporate bioinert and bioactive phases can make HSMs suitable for medical devices. HSMs with built-in chemical or electronic functionalities could be designed for energy applications, including thermal management, catalysis, and energy harvesting. The integration of HSMs in advanced manufacturing processes may revolutionize the production of high-performance materials.

In response to growing environmental concerns, research on sustainable HSMs is becoming increasingly relevant. Future studies could explore how incorporating recycled materials into HSMs affects mechanical performance and how these materials perform under environmentally demanding conditions. Additionally, developing biodegradable or recyclable HSMs could contribute to more sustainable material cycles, particularly for disposable or short-lifetime applications.

Lastly, the current drawbacks of HSMs should be considered either during service material selection or seeking improved materials designs. Despite their promising mechanical performance and multifunctional potential, several key challenges limit their widespread adoption in industrial and multidisciplinary applications. The design and fabrication of HSMs require precise control over microstructural heterogeneities, including grain size fractions, zone distributions, and interfacial properties, making large-scale production complex. Furthermore, their thermal stability is often inadequate at high temperatures due to grain growth and recrystallization in the harder (commonly nano-grained) regions, which diminishes their mechanical advantages. Very high mechanical incompatibility between soft and hard zones can lead to issues such as stress concentration, interfacial delamination, and premature failure under cyclic loading or extreme conditions. Additionally, phenomena such as the Bauschinger effect, significant springback during forming, and strain localization pose difficulties in processing and application.

Author contributions

Liliana Romero-Resendiz contributed toward writing original draft and conceptualization. Muhammad Naeem contributed toward conceptualization and review & editing.

Funding

This work was supported by the HORIZON EUROPE programme of research and innovation of the European Union evaluated under the Marie Sklodowska-Curie Actions and financed by the UK Research and Innovation, grant agreement No EP/Y020545/1.

Data availability

Not applicable.

Code availability

Not applicable.

Declarations

Conflict of interest On behalf of all authors, the corresponding author states that there is no conflict of interest.

Open Access

References

1. E.O. Hall, The deformation and ageing of mild steel: III. Discussion of results. Proc. Phys. Soc. London Sect. B **64**, 747–753 (1951). https://doi.org/10.1088/0370-1301/64/9/303
2. N.J. Petch, The cleavage strength of polycrystals. J. Iron Steel Inst. **174**, 25–28 (1953)
3. R.W. Armstrong, F.J. Zerilli, Dislocation mechanics aspects of plastic instability and shear banding. Mech. Mater. **17**, 319–327 (1994). https://doi.org/10.1016/0167-6636(94)90069-8
4. R.W. Armstrong, Engineering science aspects of the Hall–Petch relation. Acta Mech. **225**, 1013–1028 (2014). https://doi.org/10.1007/s00707-013-1048-2
5. M.F. Ashby, The deformation of plastically non-homogeneous materials. Philos. Mag. A J. Theor. Exp. Appl. Phys. **21**, 399–424 (1970). https://doi.org/10.1080/14786437008238426
6. F.R.N. Nabarro, Z.S. Basinski, D.B. Holt, The plasticity of pure single crystals. Adv. Phys. **13**, 193–323 (1964). https://doi.org/10.1080/00018736400101031
7. G.I. Taylor, The mechanism of plastic deformation of crystals. Part I—Theoretical. Proc. R. Soc. Lond. Ser. A **145**, 362–387 (1934). https://doi.org/10.1098/rspa.1934.0106
8. S.N. Naik, The Hall–Petch and inverse Hall–Petch relations and the hardness of nanocrystalline metals. J. Mater. Sci. **55**, 2661–2681 (2020). https://doi.org/10.1007/s10853-019-04160-w
9. C.S. Pande, K.P. Cooper, Nanomechanics of Hall–Petch relationship in nanocrystalline materials. Prog. Mater. Sci. **54**, 689–706 (2009). https://doi.org/10.1016/j.pmatsci.2009.03.008
10. K.A. Padmanabhan, S. Sripathi, H. Hahn, H. Gleiter, Inverse Hall–Petch effect in quasi- and nanocrystalline materials. Mater. Lett. **133**, 151–154 (2014)

11. J.H. Schneibel, M. Heilmaier, Hall–Petch breakdown at elevated temperatures. Mater. Trans. **55**, 44–51 (2015). https://doi.org/10.2320/matertrans.MA201309
12. H. Pan, Y. He, X. Zhang, Interactions between dislocations and boundaries during deformation. Materials **14**, 1–48 (2021). https://doi.org/10.3390/ma14041012
13. R.W. Armstrong, Q. Li, Dislocation mechanics of high-rate deformations. Metall. Mater. Trans. A Phys. Metall. Mater. Sci. **46**, 4438–4453 (2015). https://doi.org/10.1007/s11661-015-2779-6
14. R.W. Armstrong, S.M. Walley, High strain rate properties of metals and alloys. Int. Mater. Rev. **53**, 105–128 (2008). https://doi.org/10.1179/174328008X277795
15. S. Sin, Z. Hoe, Z. Wu, Y. Wei, The inverse Hall–Petch relation in nanocrystalline metals: a discrete dislocation dynamics analysis. J. Mech. Phys. Solids **88**, 252–266 (2016). https://doi.org/10.1016/j.jmps.2015.12.012
16. Z.D. Sha, S.S. Quek, Q.X. Pei, Z.S. Liu, T.J. Wang, V.B. Shenoy, Y.W. Zhang, Inverse pseudo Hall–Petch relation in polycrystalline graphene. Sci. Rep. **4**, 7–12 (2014). https://doi.org/10.1038/srep05991
17. M.A. Meyers, O. Vöhringer, V.A. Lubarda, The onset of twinning in metals: a constitutive description. Acta Mater. **49**, 4025–4039 (2001). https://doi.org/10.1016/S1359-6454(01)00300-7
18. Y. Zhu, K. Ameyama, P.M. Anderson, I.J. Beyerlein, H. Gao, H.S. Kim, E. Lavernia, S. Mathaudhu, H. Mughrabi, R.O. Ritchie, N. Tsuji, X. Zhang, X. Wu, Heterostructured materials: superior properties from hetero-zone interaction. Mater. Res. Lett. **9**, 1–31 (2021). https://doi.org/10.1080/21663831.2020.1796836
19. L. Romero-Resendiz, M. El-Tahawy, T. Zhang, M.C. Rossi, D.M. Marulanda-Cardona, T. Yang, V. Amigó-Borrás, Y. Huang, H. Mirzadeh, I.J. Beyerlein, J.C. Huang, T.G. Langdon, Y.T. Zhu, Heterostructured stainless steel: properties, current trends, and future perspectives. Mater. Sci. Eng. R. Rep. **150**, 100691 (2022). https://doi.org/10.1016/j.mser.2022.100691
20. K. Boufala, S. Ouhenia, G. Louis, D. Betrancourt, D. Chicot, I. Belabbas, Microstructure analysis and mechanical properties by instrumented indentation of Charonia Lampas Lampas shell. J. Mech. Behav. Biomed. Mater. **89**, 114–121 (2019). https://doi.org/10.1016/j.jmbbm.2018.09.018
21. S.J. Walden, W. Rowe, J. Mulville, S.L. Evans, P. Zioupos, Quantifying microcracks on fractured bone surfaces—potential use in forensic anthropology. J. Mech. Behav. Biomed. Mater. **142**, 105824 (2023). https://doi.org/10.1016/j.jmbbm.2023.105824
22. C. Tan, Y. Chew, R. Duan, F. Weng, S. Sui, F.L. Ng, Z. Du, G. Bi, Additive manufacturing of multi-scale heterostructured high-strength steels. Mater. Res. Lett. **9**, 291–299 (2021). https://doi.org/10.1080/21663831.2021.1904299
23. Z. Li, Y. Hu, T. Chen, X. Wang, P. Liu, Y. Lu, Microstructural evolution and mechanical behavior of thermally aged cast duplex stainless steel. Materials **13**, 5636 (2020). https://doi.org/10.3390/ma13245636
24. K. Edalati, A.Q. Ahmed, S. Akrami, K. Ameyama, V. Aptukov, R.N. Asfandiyarov, M. Ashida, V. Astanin, A. Bachmaier, V. Beloshenko, E.V. Bobruk, K. Bryła, J.M. Cabrera, A.P. Carvalho, N.Q. Chinh, I.-C. Choi, R. Chulist, J.M. Cubero-Sesin, G. Davdian, M. Demirtas, S. Divinski, K. Durst, J. Dvorak, P. Edalati, S. Emura, N.A. Enikeev, G. Faraji, R.B. Figueiredo, R. Floriano, M. Fouladvind, D. Fruchart, M. Fuji, H. Fujiwara, M. Gajdics, D. Gheorghe, Ł Gondek, J.E. González-Hernández, A. Gornakova, T. Grosdidier, J. Gubicza, D. Gunderov, L. He, O.F. Higuera, S. Hirosawa, A. Hohenwarter, Z. Horita, J. Horky, Y. Huang, J. Huot, Y. Ikoma, T. Ishihara, Y. Ivanisenko, J. Jang, A.M. Jorge, M. Kawabata-Ota, M. Kawasaki, T. Khelfa, J. Kobayashi, L. Kommel, A. Korneva, P. Kral, N. Kudriashova, S. Kuramoto, T.G. Langdon, D.-H. Lee, V.I. Levitas, C. Li, H.-W. Li, Y. Li, Z. Li, H.-J. Lin, K.-D. Liss, Y. Liu, D.M.M. Cardona, K. Matsuda, A. Mazilkin, Y. Mine, H. Miyamoto, S.-C. Moon, T. Müller, J.A. Muñoz, MYu. Murashkin, M. Naeem, M. Novelli, D. Olasz, R. Pippan, V.V. Popov, E.N. Popova, G. Purcek, P. de Rango, O. Renk, D. Retraint, Á. Révész, V. Roche, P. Rodriguez-Calvillo, L. Romero-Resendiz, X. Sauvage, T. Sawaguchi, H. Sena, H. Shahmir, X. Shi, V. Sklenicka, W. Skrotzki, N. Skryabina, F. Staab, B. Straumal, Z. Sun, M. Szczerba, Y. Takizawa, Y. Tang, R.Z. Valiev, A. Vozniak, A. Voznyak, B. Wang, J.T. Wang, G. Wilde, F. Zhang, M. Zhang, P. Zhang, J. Zhou, X. Zhu, Y.T. Zhu, Severe plastic deformation for producing superfunctional ultrafine-grained and heterostructured materials: an interdisciplinary review. J. Alloys Compd. **1002**, 174667 (2024). https://doi.org/10.1016/j.jallcom.2024.174667
25. Y. Zhu, X. Wu, Heterostructured materials. Prog. Mater. Sci. **131**, 101019 (2023). https://doi.org/10.1016/j.pmatsci.2022.101019
26. L. Romero-Resendiz, M. Naeem, Y.T. Zhu, Heterostructured materials by severe plastic deformation: overview and perspectives. Mater. Trans. (2023). https://doi.org/10.2320/matertrans.MT-MF2022010
27. X.W. Yuntian Zhu, Heterostructured materials. Prog. Mater. Sci. **131**, 101019 (2023). https://doi.org/10.1016/j.pmatsci.2022.101019
28. Y. Zhu, X. Wu, Perspective on hetero-deformation induced (HDI) hardening and back stress. Mater. Res. Lett. **7**, 393–398 (2019). https://doi.org/10.1080/21663831.2019.1616331
29. X. Wu, Y. Zhu, *Heterostructured materials: novel materials with unprecedented mechanical properties*, 1st edn. (Jenny Stanford, New York, 2021)
30. X.L. Wu, P. Jiang, L. Chen, J.F. Zhang, F.P. Yuan, Y.T. Zhu, Synergetic strengthening by gradient structure. Mater. Res. Lett. **2**, 185–191 (2014). https://doi.org/10.1080/21663831.2014.935821

31. D. Wu, M. Hao, T. Zhang, Z. Wang, J. Wang, G. Rao, L. Zhang, C. Ding, K. Zhou, L. Liu, D. Wang, Y. Wang, Heterostructures enhance simultaneously strength and ductility of a commercial titanium alloy. Acta Mater. (2023). https://doi.org/10.1016/j.actamat.2023.119182
32. J. Nie, Y. Chen, L. Song, Y. Fan, Y. Cao, K. Xie, S. Liu, X. Liu, Y. Zhao, Y. Zhu, Enhancing strength and ductility of Al-matrix composite via a dual-heterostructure strategy. Int. J. Plast. **171**, 103825 (2023). https://doi.org/10.1016/j.ijplas.2023.103825
33. L. Zhao, W. Zheng, Y. Hu, Q. Guo, D. Zhang, Heterostructured metal matrix composites for structural applications: a review. J. Mater. Sci. **59**, 9768–9801 (2024). https://doi.org/10.1007/s10853-023-09300-x
34. K. Hajizadeh, H. Maleki-Ghaleh, A. Arabi, Y. Behnamian, E. Aghaie, A. Farrokhi, M.G. Hosseini, M.H. Fathi, Corrosion and biological behavior of nanostructured 316L stainless steel processed by severe plastic deformation. Surf. Interface Anal. **47**, 978–985 (2015). https://doi.org/10.1002/sia.5806
35. J. Li, Q. Mao, M. Chen, W. Qin, X. Lu, T. Liu, D. She, J. Kang, G. Wang, X. Zhu, Y. Li, Enhanced pitting resistance through designing a high-strength 316L stainless steel with heterostructure. J. Market. Res. **10**, 132–137 (2021). https://doi.org/10.1016/j.jmrt.2020.12.005
36. Y.B. Lei, Z.B. Wang, B. Zhang, Z.P. Luo, J. Lu, K. Lu, Enhanced mechanical properties and corrosion resistance of 316L stainless steel by pre-forming a gradient nanostructured surface layer and annealing. Acta Mater. **208**, 116773 (2021). https://doi.org/10.1016/j.actamat.2021.116773
37. L. Romero-Resendiz, H.J. Kong, T. Zhang, H. Ni, S. Chen, M. Naeem, Y.T. Zhu, Achieving antimicrobial and superior mechanical properties in a scalable and cost-effective heterostructured stainless steel. Mater. Sci. Eng. A **886**, 145676 (2023). https://doi.org/10.1016/j.msea.2023.145676
38. X. Sun, F. Chen, H. Huang, J. Lin, X. Tang, Effects of interfaces on the helium bubble formation and radiation hardening of an austenitic stainless steel achieved by additive manufacturing. Appl. Surf. Sci. **467–468**, 1134–1139 (2019). https://doi.org/10.1016/j.apsusc.2018.10.268
39. G. Meric de Bellefon, K.M. Bertsch, M.R. Chancey, Y.Q. Wang, D.J. Thoma, Influence of solidification structures on radiation-induced swelling in an additively-manufactured austenitic stainless steel. J. Nucl. Mater. **523**, 291–298 (2019). https://doi.org/10.1016/j.jnucmat.2019.06.012
40. S.W. Baek, E.J. Song, J.H. Kim, M. Jung, U.B. Baek, S.H. Nahm, Hydrogen embrittlement of 3-D printing manufactured austenitic stainless steel part for hydrogen service. Scr. Mater. **130**, 87–90 (2017). https://doi.org/10.1016/j.scriptamat.2016.11.020
41. D. Kong, C. Dong, X. Ni, L. Zhang, H. Luo, R. Li, L. Wang, C. Man, X. Li, Superior resistance to hydrogen damage for selective laser melted 316L stainless steel in a proton exchange membrane fuel cell environment. Corros. Sci. **166**, 108425 (2020). https://doi.org/10.1016/j.corsci.2019.108425
42. M. Naeem, R.J. Sánchez Cruz, M.A. Esquivel Neri, Y. Ma, V. Amigó Borrás, G. González, A.J. Knowles, W. Gong, S. Harjo, Y.T. Zhu, X.-L. Wang, L. Romero-Resendiz, Enhanced cryogenic mechanical properties of heterostructured CrCoNi multicomponent alloy: Insights from in-situ neutron diffraction. Mater. Sci. Eng. A **916**, 147374 (2024). https://doi.org/10.1016/j.msea.2024.147374
43. J. Li, Y. Cao, B. Gao, Y. Li, Y. Zhu, Superior strength and ductility of 316L stainless steel with heterogeneous lamella structure. J. Mater. Sci. **53**, 10442–10456 (2018). https://doi.org/10.1007/s10853-018-2322-4
44. X. Wu, M. Yang, F. Yuan, G. Wu, Y. Wei, X. Huang, Y. Zhu, Heterogeneous lamella structure unites ultrafine-grain strength with coarse-grain ductility. Proc. Natl. Acad. Sci. **112**, 14501–14505 (2015). https://doi.org/10.1073/pnas.1517193112
45. L.P. Kubin, A. Mortensen, Geometrically necessary dislocations and strain-gradient plasticity: a few critical issues. Scripta Mater. **48**, 119–125 (2003)
46. F. Nabarro, J.P. Hirth, *Dislocations in solids*, 1st edn. (Elsevier, North-Holland, 2007)
47. D. Wu, M. Hao, T. Zhang, Z. Wang, J. Wang, G. Rao, L. Zhang, C. Ding, K. Zhou, L. Liu, D. Wang, Y. Wang, Heterostructures enhance simultaneously strength and ductility of a commercial titanium alloy. Acta Mater. **257**, 119182 (2023). https://doi.org/10.1016/j.actamat.2023.119182
48. X. Hu, S. Jin, H. Zhou, Z. Yin, J. Yang, Y. Gong, Y. Zhu, G. Sha, X. Zhu, Bauschinger effect and back stress in gradient Cu–Ge alloy. Metall. Mater. Trans. A Phys. Metall. Mater. Sci. **48**, 3943–3950 (2017). https://doi.org/10.1007/s11661-017-4176-9
49. J. Bauschinger, Changes of the elastic limit and the modulus of elasticity on various metals. Zivilingenieur **27**, 289–348 (1881)
50. X. Liu, F. Yuan, Y. Zhu, X. Wu, Extraordinary Bauschinger effect in gradient structured copper. Scr. Mater. **150**, 57–60 (2018). https://doi.org/10.1016/j.scriptamat.2018.03.007
51. H. Kato, R. Moat, T. Mori, K. Sasaki, P. Withers, Back stress work hardening confirmed by bauschinger effect in a TRIP steel using bending tests. ISIJ Int. **54**, 1715–1718 (2014). https://doi.org/10.2355/isijinternational.54.1715
52. X. Wu, Y. Zhu, Heterogeneous materials: a new class of materials with unprecedented. Mater. Res. Lett. **5**, 527–532 (2017). https://doi.org/10.1080/21663831.2017.1343208
53. O.B. Pedersen, L.M. Brown, W.M. Stobbs, The Bauschinger effect in copper. Acta Metall. **29**, 1843–1850 (1981). https://doi.org/10.1016/0001-6160(81)90110-3
54. M. Yang, Y. Pan, F. Yuan, Y. Zhu, X. Wu, Back stress strengthening and strain hardening in gradient structure. Mater. Res. Lett. **4**, 145–151 (2016). https://doi.org/10.1080/21663831.2016.1153004

55. Z. Zhang, S.K. Vajpai, D. Orlov, K. Ameyama, Improvement of mechanical properties in SUS304L steel through the control of bimodal microstructure characteristics. Mater. Sci. Eng. A **598**, 106–113 (2014). https://doi.org/10.1016/j.msea.2014.01.023
56. C. Sawangrat, S. Kato, D. Orlov, K. Ameyama, Harmonic-structured copper: performance and proof of fabrication concept based on severe plastic deformation of powders. J. Mater. Sci. **49**, 6579–6585 (2014). https://doi.org/10.1007/s10853-014-8258-4
57. K. Park, M. Nishiyama, N. Nakada, T. Tsuchiyama, S. Takaki, Effect of the martensite distribution on the strain hardening and ductile fracture behaviors in dual-phase steel. Mater. Sci. Eng. A **604**, 135–141 (2014). https://doi.org/10.1016/j.msea.2014.02.058
58. M. Calcagnotto, Y. Adachi, D. Ponge, D. Raabe, Deformation and fracture mechanisms in fine- and ultrafine-grained ferrite/martensite dual-phase steels and the effect of aging. Acta Mater. **59**, 658–670 (2011). https://doi.org/10.1016/j.actamat.2010.10.002
59. X.L. Wu, M.X. Yang, F.P. Yuan, L. Chen, Y.T. Zhu, Combining gradient structure and TRIP effect to produce austenite stainless steel with high strength and ductility. Acta Mater. **112**, 337–346 (2016). https://doi.org/10.1016/j.actamat.2016.04.045
60. X. Ma, C. Huang, J. Moering, M. Ruppert, H.W. Höppel, M. Göken, J. Narayan, Y. Zhu, Mechanical properties of copper/bronze laminates: role of interfaces. Acta Mater. **116**, 43–52 (2016). https://doi.org/10.1016/j.actamat.2016.06.023
61. C.X. Huang, Y.F. Wang, X.L. Ma, S. Yin, H.W. Höppel, M. Göken, X.L. Wu, H.J. Gao, Y.T. Zhu, Interface affected zone for optimal strength and ductility in heterogeneous laminate. Mater. Today **21**, 713–719 (2018). https://doi.org/10.1016/j.mattod.2018.03.006
62. L. Romero-Resendiz, T.S. Cano, M. Naeem, A. Ur Rehman, E. Salamci, V.T. Mendoza, E.D. Duran, L.B. Diaz, M.U. Samalci, Mechanical and electrochemical properties comparison of additively manufactured Ti–6Al–4V alloys by electron beam melting and selective laser melting. J. Mater. Eng. Perform. (2024). https://doi.org/10.1007/s11665-024-09486-4
63. A. Chen, J. Liu, H. Wang, J. Lu, Y.M. Wang, Gradient twinned 304 stainless steels for high strength and high ductility. Mater. Sci. Eng. A **667**, 179–188 (2016). https://doi.org/10.1016/j.msea.2016.04.070
64. S. Ghosh, N. Bibhanshu, S. Suwas, K. Chatterjee, Surface mechanical attrition treatment of additively manufactured 316L stainless steel yields gradient nanostructure with superior strength and ductility. Mater. Sci. Eng. A **820**, 141540 (2021). https://doi.org/10.1016/j.msea.2021.141540
65. J. Yang, L. Xu, H. Gao, X. Li, H. Pan, B. Shu, T. Itoh, Y. Zhu, X. Zhu, Effect of global constraint on the mechanical behavior of gradient materials. Mater. Sci. Eng. A **826**, 141963 (2021). https://doi.org/10.1016/j.msea.2021.141963
66. T.H. Fang, W.L. Li, N.R. Tao, K. Lu, Revealing extraordinary intrinsic tensile plasticity in gradient nano-grained copper. Science **331**(2011), 1587–1590 (1979)
67. B. Zhang, F. Xue, S.L. Li, X.T. Wang, N.N. Liang, Y.H. Zhao, G. Sha, Non-uniform phase separation in ferrite of a duplex stainless steel. Acta Mater. **140**, 388–397 (2017). https://doi.org/10.1016/j.actamat.2017.08.044
68. M.C. Somani, M. Jaskari, S. Sadeghpour, C. Hu, R.D.K. Misra, T.T. Nyo, C. Yang, L.P. Karjalainen, Improving the yield strength of an antibacterial 304Cu austenitic stainless steel by the reversion treatment. Mater. Sci. Eng. A **793**, 139885 (2020). https://doi.org/10.1016/j.msea.2020.139885
69. A. Kisko, A.S. Hamada, J. Talonen, D. Porter, L.P. Karjalainen, Effects of reversion and recrystallization on microstructure and mechanical properties of Nb-alloyed low-Ni high-Mn austenitic stainless steels. Mater. Sci. Eng. A **657**, 359–370 (2016). https://doi.org/10.1016/j.msea.2016.01.093
70. G.S. Sun, J. Hu, B. Zhang, L.X. Du, The significant role of heating rate on reverse transformation and coordinated straining behavior in a cold-rolled austenitic stainless steel. Mater. Sci. Eng. A **732**, 350–358 (2018). https://doi.org/10.1016/j.msea.2018.07.024
71. J. He, L. Chen, Z. Guo, H. Zhi, S. Antonov, Y. Su, A novel 13Cr austenitic stainless steel with excellent mechanical properties and high hydrogen embrittlement resistance via heterostructure and TRIP effects. Mater. Sci. Eng. A **793**, 139835 (2020). https://doi.org/10.1016/j.msea.2020.139835
72. X.H. Zhao, D.W. Nie, D.S. Xu, Y. Liu, C.H. Hu, Effect of gradient nanostructures on tribological properties of 316L stainless steel with high energy ion implantation tungsten carbide. Tribol. Trans. **62**, 189–197 (2019). https://doi.org/10.1080/10402004.2018.1508797
73. S. Zherebtsov, E. Kudryavtsev, S. Kostjuchenko, S. Malysheva, G. Salishchev, Strength and ductility-related properties of ultrafine grained two-phase titanium alloy produced by warm multiaxial forging. Mater. Sci. Eng. A **536**, 190–196 (2012). https://doi.org/10.1016/j.msea.2011.12.102
74. D. Orlov, Y. Todaka, M. Umemoto, N. Tsuji, Formation of bimodal grain structures in high purity Al by reversal high pressure torsion. Scr. Mater. **64**, 498–501 (2011). https://doi.org/10.1016/j.scriptamat.2010.11.020
75. W. Yinmin, C. Mingwei, Z. Fenghua, M. En, High tensile ductility in a nanostructured metal. Nature **419**, 912 (2002)
76. H. Jin, D.J. Lloyd, Effect of a duplex grain size on the tensile ductility of an ultra-fine grained Al–Mg alloy, AA5754, produced by asymmetric rolling and annealing. Scr. Mater. **50**, 1319–1323 (2004). https://doi.org/10.1016/j.scriptamat.2004.02.021
77. M.C. Zhao, F. Yin, T. Hanamura, K. Nagai, A. Atrens, Relationship between yield strength and grain size for a bimodal structural ultrafine-grained ferrite/cementite steel. Scr. Mater.

57, 857–860 (2007). https://doi.org/10.1016/j.scriptamat.2007.06.062

78. C. Shuai, D. Li, X. Yao, X. Li, C. Gao, Additive manufacturing of promising heterostructure for biomedical applications. Int. J. Extreme Manuf. (2023). https://doi.org/10.1088/2631-7990/acded2
79. Y. Kong, K. Peng, H. Huang, Highly controllable additive manufacturing of heterostructured nickel-based composites. Int. J. Mach. Tools Manuf **195**, 104112 (2024). https://doi.org/10.1016/j.ijmachtools.2023.104112
80. G.F. Liu, T.J. Chen, Synthesis of heterogeneity-improved heterostructured 2024Al alloy with excellent synergy of strength and ductility via powder thixoforming. J. Alloys Compd. **932**, 167661 (2023). https://doi.org/10.1016/j.jallcom.2022.167661
81. X. Xu, P. Kumar, R. Cao, Q. Ye, Y. Chu, Y. Tian, Y. Li, R.O. Ritchie, Exceptional cryogenic-to-ambient impact toughness of a low carbon micro-alloyed steel with a multi-heterogeneous structure. Acta Mater. (2024). https://doi.org/10.1016/j.actamat.2024.120019
82. X. Sun, X. Hao, J. Nie, Y. Fan, Y. Chen, S. Liu, X. Liu, Y. Zhao, Microstructure and enhanced cryogenic tensile property of a heterostructured Al-AlN/Al–Mg composite fabricated by accumulative roll bonding (ARB). J. Market. Res. **21**, 532–545 (2022). https://doi.org/10.1016/j.jmrt.2022.09.037
83. F.J. Guo, L.Y. Song, Q. He, B. Yang, X.H. Zheng, Q.Y. Wang, C.X. Huang, Enhancing cryogenic tensile properties of CrCoNi medium entropy alloy via heterogeneous microstructure design. Mater Charact (2023). https://doi.org/10.1016/j.matchar.2023.112951
84. W. Su, M. Wang, F. Guo, H. Ran, Q. Cheng, Q. Wang, Y. Zhu, X. Ma, C. Huang, Heterostructure enables anomalous improvement of cryogenic mechanical properties in titanium. Acta Mater. **273**, 119982 (2024). https://doi.org/10.1016/j.actamat.2024.119982
85. J.C. Cheng, N. Li, J.Y. Huang, A.R. Cui, X.J. Zhao, Y. Cai, Q.Y. Wang, S.N. Luo, Dynamic compression responses of heterogeneous-structured CrMnFeCoNi high-entropy alloy at cryogenic temperatures. Mater. Sci. Eng. A (2024). https://doi.org/10.1016/j.msea.2023.146063
86. X. Zhang, J. Li, Q. Gong, C. Liu, J. Li, Deformation behaviors at cryogenic temperature of lean duplex stainless steel with heterogeneous structure prepared by a short process. J. Market. Res. **24**, 9273–9291 (2023). https://doi.org/10.1016/j.jmrt.2023.05.093
87. Z. Zhang, W. Wang, S. Qin, M. Yang, J. Wang, P. Jiang, F. Yuan, X. Wu, Dual heterogeneous structured medium-entropy alloys showing a superior strength-ductility synergy at cryogenic temperature. J. Market. Res. **17**, 3262–3276 (2022). https://doi.org/10.1016/j.jmrt.2022.02.078
88. M. Naeem, H. He, S. Harjo, T. Kawasaki, W. Lin, J.J. Kai, Z. Wu, S. Lan, X.L. Wang, Temperature-dependent hardening contributions in CrFeCoNi high-entropy alloy. Acta Mater. **221**, 117371 (2021). https://doi.org/10.1016/j.actamat.2021.117371
89. L. Romero-Resendiz, Y. Huang, A.J. Knowles, J. Kelleher, T.L. Lee, T. Mousavi, M. Naeem, Exceptional strength–ductility combination of heterostructured stainless steel for cryogenic applications. Scr. Mater. **258**, 116527 (2025). https://doi.org/10.1016/j.scriptamat.2024.116527
90. G.B. Olson, M. Cohen, A mechanism for the strain-induced nucleation of martensitic transformations. J. Less Common Metals **28**, 107–118 (1972). https://doi.org/10.1016/0022-5088(72)90173-7
91. M. Naeem, H. He, F. Zhang, H. Huang, S. Harjo, T. Kawasaki, B. Wang, S. Lan, Z. Wu, F. Wang, Y. Wu, Z. Lu, Z. Zhang, C.T. Liu, X.L. Wang, Cooperative deformation in high-entropy alloys at ultralow temperatures. Sci. Adv. (2020). https://doi.org/10.1126/sciadv.aax4002
92. D.C.C. Magalhães, A.M. Kliauga, M. Ferrante, V.L. Sordi, Plastic deformation of FCC alloys at cryogenic temperature: the effect of stacking-fault energy on microstructure and tensile behaviour. J. Mater. Sci. **52**, 7466–7478 (2017). https://doi.org/10.1007/s10853-017-0979-8
93. M. Naeem, H. Zhou, H. He, S. Harjo, T. Kawasaki, S. Lan, Z. Wu, Y. Zhu, X.L. Wang, Martensitic transformation in CrCoNi medium-entropy alloy at cryogenic temperature. Appl. Phys. Lett. (2021). https://doi.org/10.1063/5.0067268
94. M. Naeem, H. He, S. Harjo, T. Kawasaki, F. Zhang, B. Wang, S. Lan, Z. Wu, Y. Wu, Z. Lu, C.T. Liu, X.L. Wang, Extremely high dislocation density and deformation pathway of CrMnFeCoNi high entropy alloy at ultralow temperature. Scr. Mater. **188**, 21–25 (2020). https://doi.org/10.1016/j.scriptamat.2020.07.004
95. T.S. Byun, N. Hashimoto, K. Farrell, Temperature dependence of strain hardening and plastic instability behaviors in austenitic stainless steels. Acta Mater. **52**, 3889–3899 (2004). https://doi.org/10.1016/j.actamat.2004.05.003
96. M. Yuemin, M. Naeem, L. Zhu, H. He, X. Sun, Z. Yang, H. Feng, S. Harjo, T. Kawasaki, X. Wang, Microscopic insights of the extraordinary work-hardening due to phase transformation. Acta Mater. **270**, 119822 (2024). https://doi.org/10.1016/j.actamat.2024.119822
97. K.Z. Zhou, C. Su, Y. Bao, A paradox of price–quality and market efficiency: a comparative study of the US and China markets. Int. J. Res. Mark. **19**, 349–365 (2002). https://doi.org/10.1016/S0167-8116(02)00096-4
98. X.T. Fang, G.Z. He, C. Zheng, X.L. Ma, D. Kaoumi, Y.S. Li, Y.T. Zhu, Effect of heterostructure and hetero-deformation induced hardening on the strength and ductility of brass. Acta Mater. **186**, 644–655 (2020). https://doi.org/10.1016/j.actamat.2020.01.037

99. A. Charpentier Poncelet, C. Helbig, P. Loubet, A. Beylot, S. Muller, J. Villeneuve, B. Laratte, A. Thorenz, A. Tuma, G. Sonnemann, Losses and lifetimes of metals in the economy. Nat. Sustain. **5**, 717–726 (2022). https://doi.org/10.1038/s41893-022-00895-8
100. R. Yokoi, T. Watari, M. Motoshita, Future greenhouse gas emissions from metal production: Gaps and opportunities towards climate goals. Energy Environ. Sci. **15**, 146–157 (2022). https://doi.org/10.1039/d1ee02165f
101. K. Li, J. Yang, Y. Yi, X. Liu, Y. Liu, L.C. Zhang, W. Zhang, W. Li, D. Chen, S. Zhou, Enhanced strength-ductility synergy and mechanisms of heterostructured Ti6Al4V–Cu alloys produced by laser powder bed fusion. Acta Mater. **256**, 119112 (2023). https://doi.org/10.1016/j.actamat.2023.119112
102. X. Dong, B. Gao, L. Xiao, J. Hu, M. Xu, Z. Li, J. Meng, X. Han, H. Zhou, Y. Zhu, Heterostructured metallic structural materials: research methods, properties, and future perspectives. Adv. Funct. Mater. **2410521**, 1–34 (2024). https://doi.org/10.1002/adfm.202410521
103. A. Sajeev, M. Perumalsamy, V. Elumalai, A. Sathyaseelan, S.A. Ayyappan, M. Anithkumar, S.J. Kim, Harnessing wind energy for ultraefficient green hydrogen production with tin selenide/tin telluride heterostructures. Small Sci. (2024). https://doi.org/10.1002/smsc.202300222
104. G.D. Park, J.S. Park, J.K. Kim, Y.C. Kang, Recent advances in heterostructured anode materials with multiple anions for advanced alkali-ion batteries. Adv. Energy Mater. **11**, 1–46 (2021). https://doi.org/10.1002/aenm.202003058
105. J. Du, M. Guo, T. Wang, X. Chen, D. Qiao, W. Zhou, L. Zhuang, H. Lou, Effect of heterostructure with hard/soft micro-regions on the mechanical properties and corrosion resistance of Al–Mg–Si–Cu–Zn alloys. Mater Charact (2024). https://doi.org/10.1016/j.matchar.2024.114272
106. L. Li, L. Xiao, D. Zhang, Z. Sun, B. Gao, K. Wei, Y. Yu, X. Chen, H. Zhou, Ductilization of a diffusion-bonded heterostructured AZ31/GW103K/AZ31 alloy by interfacial reinforcement. Mater. Sci. Eng. A **852**, 143691 (2022). https://doi.org/10.1016/j.msea.2022.143691
107. W. Ai, Y. Lin, F. Chen, Microstructure and mechanical properties of Ti–Mg lightweight heterostructured materials. Mater. Sci. Eng. A **850**, 143560 (2022). https://doi.org/10.1016/j.msea.2022.143560
108. K. Wei, J. Li, W. Cheng, W. Qin, W. Jiang, Z. Li, Y. Zhao, A. Meng, X. Sun, Q. Mao, Remarkable cryogenic tensile property of the 304L stainless steel with a lamellar bimodal heterostructure. J. Mater. Sci. **59**, 14065–14077 (2024). https://doi.org/10.1007/s10853-024-10037-4
109. Y. Li, J. Yang, R. Zhao, Y. Zhang, X. Wang, X. He, Y. Fu, L. Zhang, Design of organic-inorganic hybrid heterostructured semiconductors via high-throughput materials screening for optoelectronic applications. J. Am. Chem. Soc. **144**, 16656–16666 (2022). https://doi.org/10.1021/jacs.2c07434
110. C. Xie, Y. Wang, Z.X. Zhang, D. Wang, L.B. Luo, Graphene/semiconductor hybrid heterostructures for optoelectronic device applications. Nano Today **19**, 41–83 (2018). https://doi.org/10.1016/j.nantod.2018.02.009
111. S.A. Al-Anezi, The effect of orthodontic bands or tubes upon periodontal status during the initial phase of orthodontic treatment. Saudi Dent. J. **27**, 120–124 (2015). https://doi.org/10.1016/j.sdentj.2014.11.010
112. E. Mizrahi, Surface distribution of enamel opacities following orthodontic treatment. Am. J. Orthod. **84**, 323–331 (1983). https://doi.org/10.1016/S0002-9416(83)90348-2
113. S. Acham, A. Truschnegg, P. Rugani, B. Kirnbauer, K.E. Reinbacher, W. Zemann, L. Kqiku, N. Jakse, Needle fracture as a complication of dental local anesthesia: recommendations for prevention and a comprehensive treatment algorithm based on literature from the past four decades. Clin. Oral Investig. **23**, 1109–1119 (2019). https://doi.org/10.1007/s00784-018-2525-8
114. S. Seon, B.-S. Lee, B. Choi, J. Ohe, J. Lee, J. Jung, B. Hwang, M. Kim, Y. Kwon, Removal of a suture needle: a case report. Maxillofac. Plast. Reconstr. Surg. **43**, 22 (2021). https://doi.org/10.1186/s40902-021-00309-3
115. M.A.J.J.C. Teixeira, L. Adidharma, G.L. Coppit, Migration of broken dental needle through the internal jugular vein in the parapharyngeal space. Mil. Med. **186**, 454–456 (2021). https://doi.org/10.1093/milmed/usaa328
116. B. Sahin, S. Yildirimturk, Y. Sirin, B. Basaran, Displacement of a broken dental injection needle into the perivertebral space. J. Craniofacial Surg. **28**, e474–e477 (2017). https://doi.org/10.1097/SCS.0000000000003781
117. C. Lei, X. Li, X. Deng, Z. Wang, G. Wang, Deformation mechanism and ductile fracture behavior in high strength high ductility nano/ultrafine grained Fe–17Cr–6Ni austenitic steel. Mater. Sci. Eng. A **709**, 72–81 (2018). https://doi.org/10.1016/j.msea.2017.10.043
118. H. Dong, Z.C. Li, M.C. Somani, R.D.K. Misra, The significance of phase reversion-induced nanograined/ultrafine-grained (NG/UFG) structure on the strain hardening behavior and deformation mechanism in copper-bearing antimicrobial austenitic stainless steel. J. Mech. Behav. Biomed. Mater. **119**, 104489 (2021). https://doi.org/10.1016/j.jmbbm.2021.104489
119. C.B. Wahl, M. Aykol, J.H. Swisher, J.H. Montoya, S.K. Suram, C.A. Mirkin, Machine learning-accelerated design and synthesis of polyelemental heterostructures. Sci. Adv. **7**, 1–9 (2021). https://doi.org/10.1126/sciadv.abj5505
120. J. Jung, J.I. Yoon, H.K. Park, J.Y. Kim, H.S. Kim, Bayesian approach in predicting mechanical properties of materials: application to dual phase steels. Mater. Sci. Eng. A **743**, 382–390 (2019). https://doi.org/10.1016/j.msea.2018.11.106

121. E.M. Williamson, R.L. Brutchey, Using data-driven learning to predict and control the outcomes of inorganic materials synthesis. Inorg. Chem. **62**, 16251–16262 (2023). https://doi.org/10.1021/acs.inorgchem.3c02697
122. Y.B. Lei, Z.B. Wang, J.L. Xu, K. Lu, Simultaneous enhancement of stress- and strain-controlled fatigue properties in 316L stainless steel with gradient nanostructure. Acta Mater. **168**, 133–142 (2019). https://doi.org/10.1016/j.actamat.2019.02.008
123. C.W. Shao, P. Zhang, X.G. Wang, Q. Wang, Z.F. Zhang, High-cycle fatigue behavior of TWIP steel with graded grains: breaking the rule of mixture. Mater. Res. Lett. **7**, 26–32 (2019). https://doi.org/10.1080/21663831.2018.1550822
124. P.M. Pohl, R. Brodwolf, D. Ma, M. Göken, H.W. Höppel, Damage tolerant fatigue behavior of laminated metallic composites with dissimilar yield strength. J. Mater. Sci. **60**, 939–963 (2025). https://doi.org/10.1007/s10853-024-10550-6
125. S. Kikuchi, T. Imai, H. Kubozono, Y. Nakai, M. Ota, A. Ueno, K. Ameyama, Effect of harmonic structure design with bimodal grain size distribution on near-threshold fatigue crack propagation in Ti–6Al–4V alloy. Int. J. Fatigue **92**, 616–622 (2016). https://doi.org/10.1016/j.ijfatigue.2016.02.038
126. P.C. Han, Q. Li, N.R. Tao, Strain partition induced abnormal low-cycle fatigue behavior in single-phase heterostructured 316L stainless steels. Scr. Mater. **227**, 115274 (2023). https://doi.org/10.1016/j.scriptamat.2022.115274